AFCRL-63-451

THERMIONIC EMISSION FROM METAL CRYSTALS IN ALKALI METAL VAPORS

H. F. Webster and P. L. Read

General Electric Company
Research Laboratory
Schenectady, New York

Contract No. AF-19(604)-8424

Project No. 8659

Task No. 865902

Scientific Report No. 2

May 1963

Prepared

for

AIR FORCE CAMBRIDGE RESEARCH LABORATORIES
OFFICE OF AEROSPACE RESEARCH
UNITED STATES AIR FORCE
BEDFORD, MASSACHUSETTS

Requests for additional copies by Agencies of the Department of Defense, their contractors, and other Government agencies should be directed to the:

DEFENSE DOCUMENTATION CENTER
ARLINGTON HALL STATION
ARLINGTON 12, VIRGINIA

All other persons and organizations should apply to the:

U.S. DEPARTMENT OF COMMERCE
OFFICE OF TECHNICAL SERVICES
WASHINGTON 25, D. C.

ABSTRACT

Thermionic emission microscopes have been used to evaluate the emission density from tungsten, molybdenum, tantalum, niobium, nickel, rhenium, and niobium carbide in cesium, rubidium, and potassium vapors as a function of alkali vapor pressure, emitter temperature, and emitter crystal face. It was found that when the emitter surface had less than a monolayer coverage of alkali metal, it was the atomically closest packed plane of the emitter which yielded the highest thermionic emission density. The effects of surface contaminants were studied and evidence was obtained suggesting that the high work function of the 112 plane of tungsten and molybdenum may be caused by a contaminant.

Manuscript received May 10, 1963.

TABLE OF CONTENTS

LIST OF ILLUSTRATIONS

LIST OF ILLUSTRATIONS (CONT'D.)

THERMIONIC EMISSION FROM METAL CRYSTALS IN ALKALI METAL VAPORS*

H. F. Webster and P. L. Read

I. INTRODUCTION

It has been known for some time that the work function of a metal crystal coated with thin films of cesium or other electropositive elements depends upon the lattice structure of the metal crystal. The existence of this anisotropy was found in the Nineteen Thirties after the development of various electron microscope techniques and it was observed both in thermionic emission and in field emission. Bruche[1] observed differences in thermionic emission from various grains of a polycrystalline nickel sample coated with cesium. Johnson and Shockley[2] used a cylindrical thermionic microscope to observe emission differences from different crystal faces of tungsten coated with cesium, potassium, and thorium. This geometry gives magnification in one dimension only, and an improved microscope was made by Martin[3] who used a spherical tungsten cathode in both cesium and barium vapors.

With the development of the field emission microscope by Müller,[4] the dependence of work function of both clean and cesium covered metals upon the crystal structure of the exposed crystal face was observed by a number of workers. A review article[5] has appeared in which photographs are reproduced of field emission patterns from alkali-covered metals in which the large variation of emission density with crystal face is apparent. Most of these investigations with both the thermionic and field emission microscopes were not quantitative, but in some experiments an effort was made to deduce the emission density from the light output of the phosphor.

This report reviews some recent work on the variations of thermionic emission density from various alkali-coated metal crystal faces performed with a spherical cathode emission microscope similar to that of Martin but modified to allow quantitative measurements of the emission current to be made.[6, 7]

The basic idea of this microscope is that a sphere cut from a single crystal of the base metal will have all possible arrangements of surface atoms exposed at various points of its surface. Thus if the local work function, or the binding of foreign atoms to a surface is dependent on the arrangement of the surface atoms, these properties will vary from point to point on the surface of the sphere. The microscope makes use of this variation by projecting a map of the electrons thermionically emitted at the sphere surface onto a planar anode surface. Thus the variations in current density at the anode can be related back to the variation in work function at the cathode sphere surface.

---

*This work is related to that performed under previous contract No. AF-19(604)-5472, reported under Scientific Report No. 6 of that contract March 1961, and published in Journal of Applied Physics, Vol. 32, p. 1802 (1961).

The microscope is similar in geometry to some of the field emission microscopes of Müller but differs in having a much larger cathode sphere. This results in a relatively small electric field strength at the sphere surface which is insufficient to remove electrons by the field emission process.

II. EXPERIMENTAL METHOD

A. Emission Microscope Tube Construction

The experiments to be described here were done with thermionic emission microscope tubes similar to the one shown in Fig. 1. This tube was similar to that described in an earlier publication,[8] but it has been modified to yield better operation under the condition of low emission current densities and to permit in some experiments the emitting sphere to operate in a beam of cesium atoms arriving from the side tube reservoir.

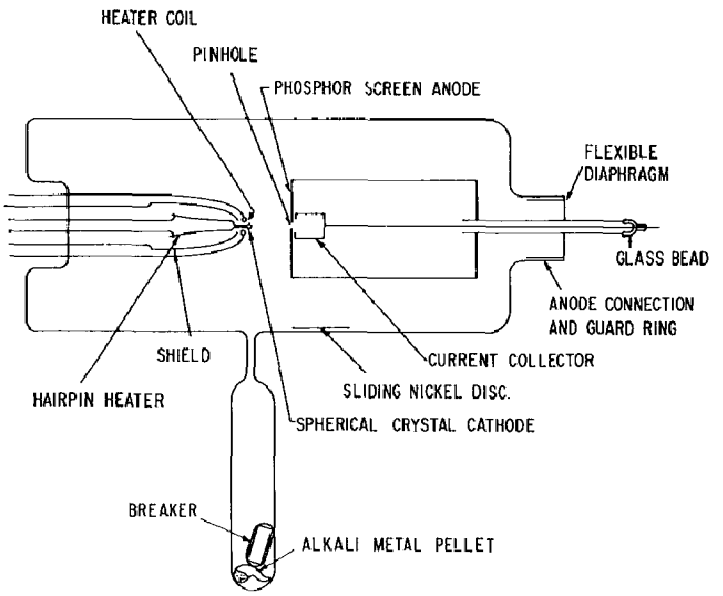

Fig. 1 Thermionic emission microscope tube.

The cathode consisted of a single-crystal sphere and the anode of a planar phosphor-coated metal disk which had a pinhole at its center. A Faraday cage current collector was located behind the pinhole in the anode. The whole anode was movable so the pinhole could be used to sample the emission current density from various parts of the emitting ball. The cathode was heated by the hairpin heater and the shield prevented electrons emitted by the heater from reaching the anode. The single-turn auxiliary heater was used to heat by electron bombardment the cathode ball to very high temperatures in order to clean it. The tube of Fig. 1 differed from the earlier version in having the current collector electrode supported entirely from the single glass bead. When the tube was being operated, this glass bead was kept warmer than the rest of the tube by a jet of hot air which prevented the condensation of cesium. The anode support completely surrounded this glass bead and served as a guard ring by interrupting leakage paths from the cathode to current collector. These two measures permitted currents of electrons in the 10^{-12} amp range to be measured even when the tube was filled with cesium vapor.

The tubes of most recent construction have been made with the cesium reservoir pointed at the side of the cathode ball as shown in Fig. 1. This permitted several types of experiments to be done. After the cesium pellet had been broken but before the glass walls of the tube surrounding the cathode ball had been saturated with cesium, the ball ran in a directed flux of cesium atoms from the cesium pool in the side tube. This allowed observation of the migration of cesium over the surface of the ball as the cesium moved away from the coated side. By moving the sliding nickel disk from outside the tube with a magnet, the cesium atom flux could be shuttered and the buildup time of electron emission and hence the cesium film on the ball could thus be observed. When the tube and side tube were all at the same temperature, equilibrium measurements could be made of electron and ion emission density as described in the earlier publication. (8)

The envelopes of the tubes were made of FN glass and seals were made to Fernico rods and cylinders. The flexible diaphragm which allowed motion of the anode also was made of Fernico. The phosphor screen was zinc oxide with excess zinc held to a tantalum disk by a potassium silicate binder. This phosphor screen survived prolonged exposure to cesium vapor. However, some loss of light output was observed in tubes which were several months old. Potassium was found to be more harmful than cesium to the phosphor coating and no image could be obtained without going to high voltages.

A tube was made with a tin oxide conductive coating on the tube walls and behind the phosphor coating but was not found satisfactory because the cesium darkened the layer until it was very difficult to see through it. This darkening disappeared again as soon as the layer was exposed to air.

The shield around the hairpin heater was a tantalum spinning. Both the hairpin heater and the auxiliary heater were made of the same material as the cathode ball whenever wire of that material was available and had sufficient mechanical strength at electron emitting temperatures. Exceptions to that rule were nickel, silver, and niobium carbide samples which were heated by tungsten wire heaters.

The alkali metals used in the experiments were cesium, rubidium, and potassium which had been condensed in breakable ampules by vacuum distillation. Following assembly, vacuum bakeout, and sealoff, the ampules were broken in the tube by striking them with a glass-enclosed iron slug.

B. Preparation of Cathode Spheres

The cathode samples for the emission microscope tubes have been formed in two ways: by hanging-drop method, and by machining them out of single-crystal stock. In producing these cathodes, the process used to form the final surface was of great importance since many treatments leave steps and facets of certain special crystallographic orientation. If such a surface were used, the emission would be characteristic of only the facet planes formed by that treatment instead of all the crystallographic planes which are to be measured in the experiments.

1. Hanging-Drop Method

Figure 2 shows the apparatus used to make the cathode spheres by the hanging-drop method. A rod of the cathode material of high purity was suspended in a bell jar vacuum system by a fine wire of the same material. The lower end of the rod was often tapered to a point. A bombardment heater coil, also of the same material, was placed around the rod such that it would heat the lower end hotter than the upper end. Typical operating conditions for this bombardment heater arrangement were with the rod 300 to 500 volts positive relative to the coil and 0.1 to 0.3 ampere of electron current flowing to the rod. The lower end of the rod was heated to 100° to 200°C less than the melting point of the rod material for a time of about an hour. At the end of this time the end of the rod

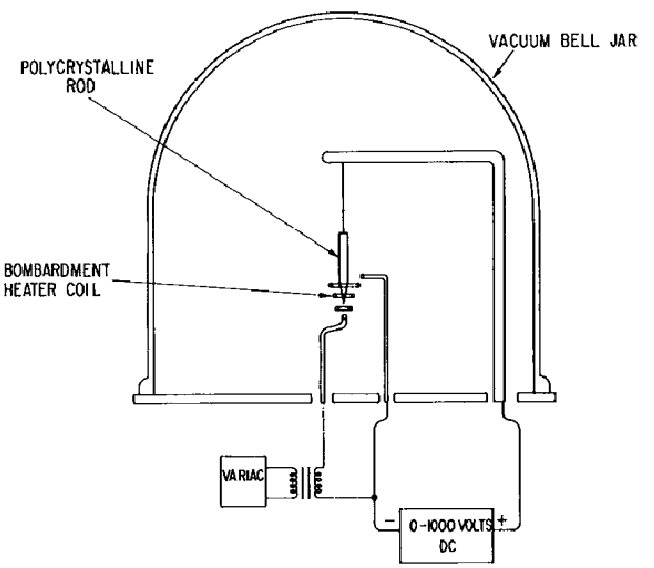

Fig. 2 Apparatus for growing single-crystal metal spheres by hanging-drop method.

was heated to the melting point and liquid drop formed and the rod was quickly cooled. In an appreciable fraction of the melts, a single-crystal or bicrystal-spherical ball resulted. In order for this to happen, it was necessary that during the hour heating period, the lower end of the rod recrystallized in one or two large grains. Thus when the liquid hanging-drop formed it seeded on these grains and froze in single- or double-crystal form. Figure 3 shows a tantalum rod and sphere formed by this method.

It was important that the ball be cooled down quickly after it had frozen as prolonged heating of the ball at temperatures near the melting point resulted in a faceted structure. All the balls used in these experiments initially were excellent spherical mirrors and they showed no facets under the highest optical magnification available. Figure 4 is included to illustrate the mirror surface finish. It was taken by viewing the reflection of a card bearing the words "single crystal" in a molybdenum sphere under the microscope.

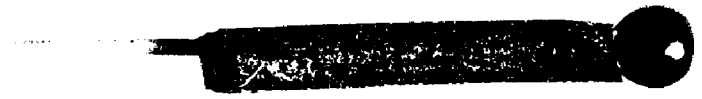

Fig. 3 Tantalum rod and sphere.

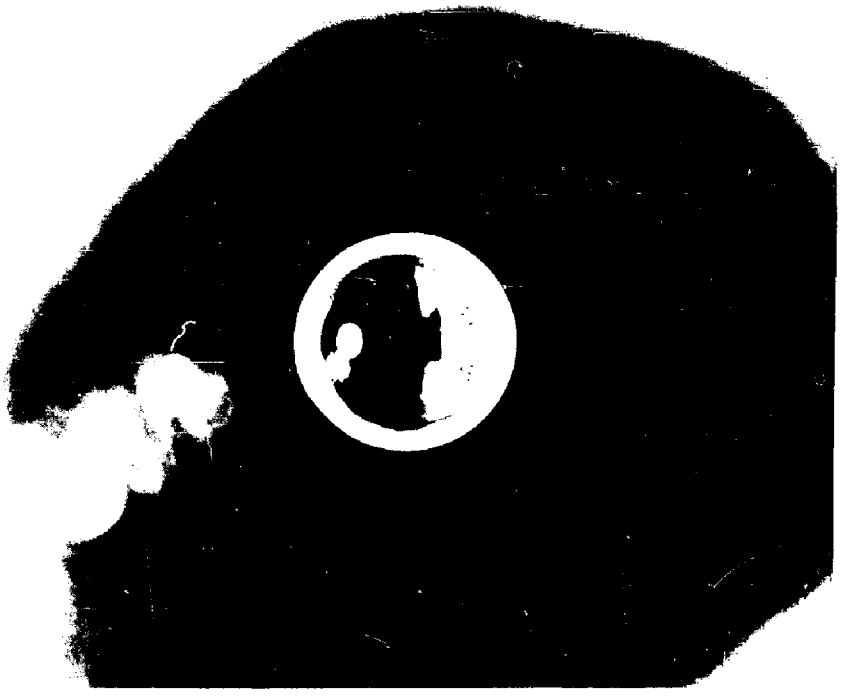

Fig. 4 Mirror surface finish.

The hanging-drop method usually produced spherical surfaces due to surface tension in the liquid drop; however, occasionally the ball would have a dimple and sometimes the surface would show ripples as if the liquid ball were oscillating at the moment it froze. The most usual cause of failure of the method, however, was insufficient grain growth in the rod which would produce balls consisting of 10 or more grains. Emission microscope experiments performed with balls of 2 or 3 grains, however, were of interest, since they gave information on the effects of grain boundaries on emission properties.

The hanging-drop method was used successfully with tungsten, tantalum, molybdenum, niobium, rhenium, and platinum. The method was less successful when tried with iridium, rhodium, and nickel, although it might have been successful with different initial sample rods.

There are two reasons for starting with material of high purity. It is known that certain impurities inhibit the motion of grain boundaries, and thus it would be difficult to grow large grains in the rod and so produce single-crystal

spheres. The second reason is the obvious one that one would like as pure and clean a cathode sample as can be obtained because impurities may affect the electron emission or cesium adsorption properties. One of the advantages of the hanging-drop method is that many of the impurities which might be present in the material are rapidly ejected when the material is heated to temperatures near or above the melting point.

One difficulty with the hanging-drop method was encountered with the less refractory metals. As previously mentioned, the bombardment heater coil was always made of the same material as the sample being formed. Thus any evaporation from the heater would not contaminate the sample. Materials such as Pt, Ir, Ni, and Rh, however, are not mechanically strong enough at their electron-emitting temperature to make self-supporting coils and so for these materials tungsten bombardment coils were used. As a result, it is possible that some tungsten could be present in those particular samples.

2. Machining and Electropolishing Method

Whenever single-crystal stock is available, the cathode spheres can be made by machining them out of a large piece. A major problem with this method, however, is getting rid of the surface layer left by the machining. The machine tool leaves behind a layer of small crystallites of random orientation which overlays the single-crystal material below.

The method used most successfully here is that of high-voltage electrolytic etching. Generally neither low-voltage electrolytic etching nor chemical etching can be used because both of these methods selectively attack various crystallographic planes and result in faceted structures which as previously indicated are not suitable for these experiments. Figure 5 shows a silver single-crystal ball which has been etched in dilute nitric acid. The variations of reflectivity associated with the facets can be seen. The center of the triangular region is a 111 direction.

When electrolytic etching is used with 1 to 2 volts across the solution, this voltage is comparable with the work function difference between the various crystal planes and marked differences between rate of attack on the different crystal planes are observed. When the applied voltage is 10 volts or more the attack rate appears to depend more upon the surface geometry and points are removed leaving smoothed and polished surfaces. This is the method that was used with all the machined samples.

In order to use this method, however, it is necessary to find an electrolyte which does not attack the surface chemically before the voltage is applied, or if chemical attack does occur, it must be very slow relative to the electrolytic action. The bath used for nickel was two parts of methanol and one part of concentrated nitric acid. The bath for niobium carbide was two parts of lactic acid, one part of sulphuric acid, and one part of hydrofluoric acid. Certain cyanide baths are suitable for silver. It should be remembered that the solutions for all these metals may be explosive, poisonous, or corrosive and one would be well advised to consult some of the references on etching[9] before using them.

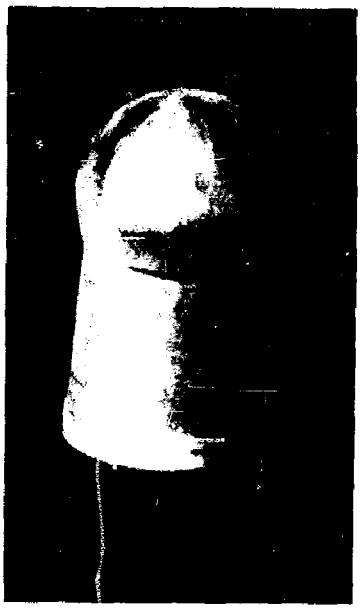

Fig. 5 Silver single-crystal ball etched in dilute nitric acid.

C. The Projection of the Electron Microscope Image

1. Relation to Stereographic Projection

Electrons leaving the cathode sphere initially are accelerated away from it in a radial direction by the radial electric field in that region. Their paths then turn and they strike the anode phosphor screen giving an enlarged map of the emission current variations at the sphere. It is important to know the way the image projects since this enables one to relate current densities at the anode back to the various crystallographic planes at the surface of the sphere from which they came. This microscope projection turns out to be very close to a stereographic projection. It is more complicated, however, because electrons from the back side of the ball also reach the screen and give a double-valued ring around its outer edge.

Figure 6 shows a stereographic projection for a cubic crystal with the 110 direction at its center. The basic triangle with the 110, 100, and 111 directions at its vertices contains all possible crystallographic directions, and if emission current density can be measured over this area the complete emission dependence on crystal face will be known. It will be seen that the complete pattern is highly redundant with the basic triangle being repeated 24 times. Some of the outer triangles may be confused by the double-valued pattern of the electrons from the back surface but the inner eight triangles have always been usable for measurement.

Before all of the cathode spheres were mounted in emission tubes they were x-rayed to establish their orientation. The observed emission patterns, however, always have had such obvious symmetry properties that all of the low Miller index directions could be immediately established by inspection. When locating some of the higher index planes, more careful attention to the projection was required.

The potentials applied to the shield and single-turn bombardment heater may be adjusted to determine the size of the pattern and the position of the double-valued ring. Once these potentials had been determined, they were established by connecting the various electrodes to a series resistor string. In this way when the cathode-anode voltage was varied, the other electrode voltages varied in the same proportion and the pattern size and shape remained unchanged. An exception to this occurred in some tubes in which electrons could strike the glass walls and charge them. However, this was generally a small effect.

The stereographic projection can be used in the following way for interpolation in the electron emission pattern. A central spot and an outer spot are initially identified by their symmetry properties. These two are used to establish the scale

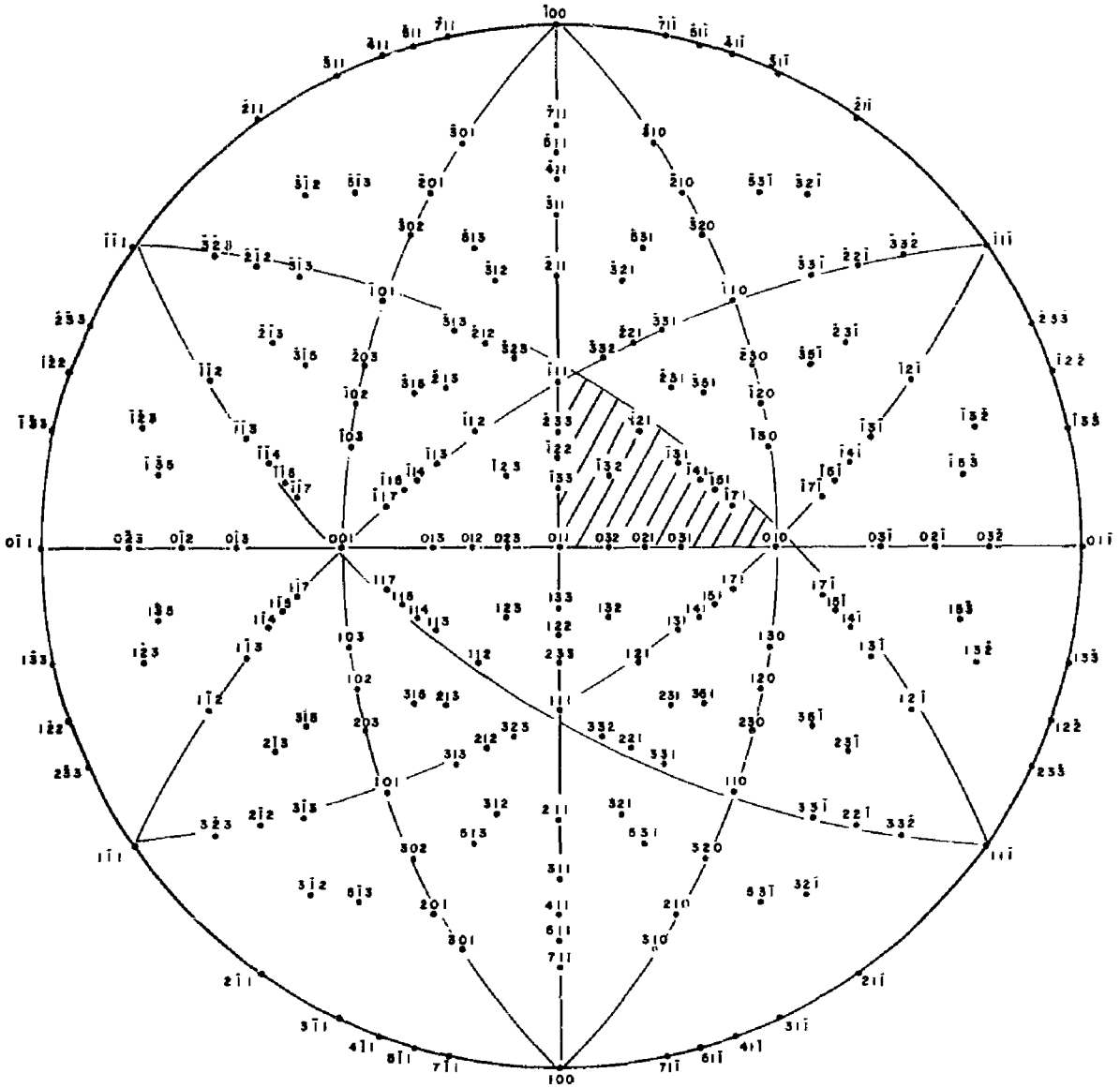

Fig. 6 Stereographic projection for a cubic crystal.

of the pattern and other spots between them can be identified by using the stereograph projection for interpolation. To check this procedure a pattern which had 100, 110, 111, and 112 spots identifiable was measured and the position of the intermediate spots was correctly predicted within the accuracy with which measurements could be made from the photograph of the pattern.

This microscope has been used not only for the projection of electron patterns but also for the projection of positive ions produced at the sphere surface by surface ionization. The positive ion currents, however, are not large enough to produce a visible image on the phosphor and all determinations of positive ion currents have to be made with the pinhole current collector. To locate the

pinhole it has been necessary to make use of the fact that the paths of particles traveling in such an electric field are independent of the mass of the particles.[10] For such positive ion measurements, the microscope is set up to produce a visible electron image and the pinhole is located at the point in the pattern where current is to be measured. The polarity of the voltage applied to the series resistor string is then reversed and the positive ion current measured. It is, of course, important that the series current in the resistor string be large compared to any of the currents flowing to the various electrodes. Then the relative potentials of the various electrodes will be unchanged by the emission currents and the pattern size and shape will be the same for electrons and ions.

2. Calculation of the Magnification of the Thermionic Emission Microscope

The raw data obtained from the thermionic emission microscope (TEM) consist of measurements of the current received by the Faraday cup current collector which lies behind the pinhole in the screen. In order to convert these data to current density at the surface of the emitter it is necessary to know how the pinhole in the screen maps back onto the surface of the single-crystal spherical emitter along the trajectories of the emitted electrons. That is, it is necessary to know the areal magnification of the TEM. In this section we shall derive an expression for the areal magnification of the TEM as a function of the initial position of the emitted electron on the emitter surface.

In order to simplify our calculation of the areal magnification of the TEM we shall consider the somewhat unrealistic model of a TEM where the emitter is considered to be an isolated, negatively charged, conducting sphere and the screen is considered to be a grounded, conducting, infinite plane. This model neglects the presence of the shank on which the emitter sphere is mounted, the shield, the bombardment filament, and the glass walls of the tube. Also neglected is the fact that the screen is not of infinite extent. Although this oversimplified model is but a rough approximation to reality, the fact that the relative potentials of the shank, shield, and bombardment filament remain fixed with respect to screen potential allows us to correct for their presence and for the finiteness of the screen by inserting an appropriate numerical correction factor into the expression for the magnification. The relative potential of the walls of the glass envelope near the screen will in general not remain fixed with respect to screen potential since the glass takes a finite time to acquire its charge. However, this effect will cause only a small perturbation on the center of the pattern (where current measurements are made) especially if the glass walls are given time to charge up close to their final potential.

The potential distribution of a negatively charged sphere a distance, a, in front of a grounded plane is exactly the same as the potential distribution between two identical conducting spheres having equal but opposite charge whose centers are a distance, 2a, apart. This latter potential distribution is similar to the well-known[11] distribution of two point charges with equal but opposite charge, placed a distance 2a apart. This similarity arises from the fact that the equipotential surfaces in the point charge system are very nearly spherical

in the region close to the point charges. Since the radius of our emitter spheres is small compared to the distance, a, we may represent our charged sphere by a point charge located close to its center which then has an equipotential surface that almost coincides with the surface of the sphere. The validity of replacing the conducting sphere by a point charge at its center is examined in the Appendix.

It is shown there that for the dimensions of the usual TEM, the equipotential surface of a point charge which almost coincides with the emitter sphere has a deviation from sphericity of less than 1 part in 10^3 and that the point charge which gives rise to this equipotential surface lies at the center of the equipotential "sphere" to within 1 part in 10^3. Since we are not able to measure either deviations from sphericity of our actual emitter or the screen-to-emitter distance with this accuracy, we may replace the charged spheres with point charges at their centers in our derivation of the areal magnification of the TEM.

The problem now consists of determining how the pinhole maps back onto a spherical equipotential surface (whose radius is equal to the emitter radius) where the electron trajectories are those between two point charges of opposite charge placed a distance 2a apart. Unfortunately, for a nonzero applied field, the electron paths will not follow the lines of force since the electrons are emitted with a finite velocity and since they gain energy from the field as they traverse the interelectrode space. These inertial effects will cause the electron trajectories to diverge outward from the particular line of force on which they started. In order to properly take these inertial effects into account one should carry out an iterative calculation using electron-optical methods.[10] Again in the interest of simplicity, we shall ignore the inertial effects in our derivation and assume that the emitted electrons will follow along lines of force.

It can be shown[10] that the trajectories of electrons emitted with zero velocity are independent of the strength of the applied electric field. Also, the effect of the nonzero initial velocities of the emitted electrons is very small at all temperatures of interest. Electrons at the maximum in the Maxwell-Boltzmann distribution corresponding to the temperature T have [12] a kinetic energy of T/11,600 ev, which is a small fraction of a volt at ordinary emitter temperatures. Thus, we may correct for these inertial effects by inserting a numerical correction factor into our derived expression for the areal magnification. The product of this factor and the numerical correction factor mentioned above can be evaluated by comparing the observed and calculated magnification in regions near the center of the screen.

The magnification derived in this zero inertia approximation will be sufficiently accurate for our purposes. However, for extremely accurate measurements of the variation of the emission with applied field strength, a more sophisticated evaluation of the TEM magnification would be needed which takes into account the initial velocity distribution of the emitted electrons.

The areal magnification derived in the zero inertia approximation will set a lower limit on the magnification of the TEM, since the inertial effects will tend to spread out the pattern and so increase the magnification. It is possible to set an upper bound on the magnification, and thus an upper limit on the error

arising from neglecting the inertial effects, by calculating the magnification in the case where the electrons are considered to possess infinite inertia. We shall carry out this simple calculation and compare it with the zero inertia calculation. [See Eqs. (11) through (14) and Fig. 8.]

Our problem is that of determining how the surface of the emitting sphere (represented by an equipotential of a point charge located at its center) maps onto the screen along the lines of force joining this point charge to its image behind the screen. The screen lies in the plane of zero potential. We shall calculate the areal magnification as a function of θ, where θ is the angle between the line normal to the screen joining the center of the sphere to the screen and the line joining the center of the sphere to the point on the sphere where the emission takes place. Then, θ defines the initial direction of the emitted electron from the emitter sphere, which, by the reasoning in the Appendix, is radially outward.

Rather than determining how the pinhole itself maps back onto the emitter sphere, let us do the equivalent problem of determining how an annular ring of thickness, dy, on the screen, where y is measured outward from the normal to the screen passing through the point charges, maps back onto the emitter sphere.

Referring to Fig. 7, the area of this annular ring A_S is

$$A_S = 2\pi y^* dy^*$$

where y^* is the value of y corresponding to the direction of emission θ^* at the surface of the sphere. The corresponding area on the sphere A_B is

$$A_B = 2\pi r_0^2 \sin\theta^* d\theta^*$$

where r_0 is the radius of the sphere. The areal magnification M is

$$M = \frac{A_S}{A_B} = \frac{1}{r_0^2 \sin\theta} \left(y \frac{dy}{d\theta} \right) . \qquad (1)$$

Thus, we must find $(y\, dy/d\theta)$ from the equations of the lines of force.

The equation of the line of force with label C is in MKS units, from Ref. 11,

$$\frac{(x + a)}{[(x + a)^2 + y^2]^{1/2}} - \frac{(x - a)}{[(x - a)^2 + y^2]^{1/2}} = C . \qquad (2)$$

Let us first find the value of y corresponding to a given value of C at the screen. Here, $x = 0$ and the line of force equation becomes

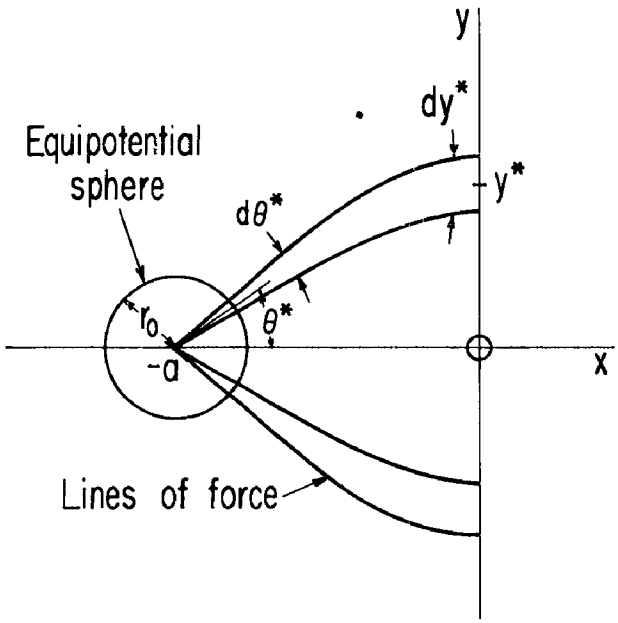

Fig. 7 Lines of force projection (in text).

$$\frac{2a}{[a^2 + y^2]^{1/2}} = C \quad ,$$

or

$$y = \pm\ a \left[\frac{4}{C^2} - 1 \right]^{1/2} \quad . \tag{3}$$

Next, we must find C as a function of θ. Starting again with Eq. (2) for the lines of force and transforming the coordinates by

$$x^\dagger = x + a$$
$$y^\dagger = y$$

so that the origin of the coordinate system will be at the center of the sphere, and transforming to polar coordinates by

$$x^\dagger = r \cos \theta$$
$$y^\dagger = r \sin \theta \, ,$$

Eq. (2) takes the form

$$\cos \theta + \frac{(2a - r \cos \theta)}{[4a^2 - 4ar \cos \theta + r^2]^{1/2}} = C \quad . \tag{4}$$

Now, we are concerned with the evaluation of C on the surface of the sphere. Here, $r \ll a$, and we may expand the denominator of Eq. (4) keeping terms up to order r^2/a^2. Thus,

$$C = \cos\theta + \left[1 - \frac{r}{2a}\cos\theta\right]\left[1 + \frac{1}{2}\left(-\frac{r}{a}\cos\theta + \frac{r^2}{4a^2}\right) + \frac{3}{8}\left(\frac{r^2}{a^2}\cos^2\theta\right)\right]$$

which reduces to

$$C = 1 + \cos\theta + \frac{r^2}{8a^2}\sin^2\theta \quad . \tag{5}$$

Now, at the surface of the sphere, $r = r_0$, and r_0 is typically about a/15. Moreover, we are usually concerned with the range of θ from 0° to 15° so that the $\sin\theta$ is also small. Under these conditions the third term in Eq. (5) is negligible so that we may write, with an accuracy of more than 0.1 per cent

$$C = 1 + \cos\theta \tag{6}$$

or in terms of half angles

$$C = 2\cos^2\frac{\theta}{2} \quad . \tag{7}$$

We may now eliminate the parameter C between Eqs. (3) and (7)

$$y = a\left[\frac{1}{\cos^4\frac{\theta}{2}} - 1\right]^{1/2} \quad . \tag{8}$$

Differentiating with respect to θ, we find

$$\frac{dy}{d\theta} = a\,\frac{\tan\frac{\theta}{2}}{\cos^4\frac{\theta}{2}}\left[\frac{1}{\cos^4\frac{\theta}{2}} - 1\right]^{-1/2}$$

and

$$y\,\frac{dy}{d\theta} = a^2\,\tan\frac{\theta}{2}\,\sec^4\frac{\theta}{2} \quad . \tag{9}$$

Finally, we may substitute this value of ($y\, dy/d\theta$) into Eq. (1)

$$M = \frac{a^2}{r_0^2} \quad \frac{\tan\frac{\theta}{2}\sec^4\frac{\theta}{2}}{\sin\theta}$$

or

$$M = \frac{a^2}{r_0^2} \quad \frac{\sec^4\frac{\theta}{2}}{(1+\cos\theta)}$$

or

$$M = \frac{a^2}{r_0^2} \quad \frac{4}{(1+\cos\theta)^3} \quad . \tag{10}$$

The areal magnification of the TEM, under the zero inertia approximation, is given by Eq. (10). The magnification M is a slowly varying function of θ for small θ as can be seen in Fig. 8.

How well does this calculated magnification agree with the magnification actually exhibited by a TEM ? It is difficult to accurately measure areal magnification but linear magnifications can be easily measured. We have carefully measured with a cathetometer the distance (0.842 cm) between the centers of two neighboring 110 spots on the screen of the W-Cs TEM tube. The great circle on the emitter sphere joining the 110 regions came very close to passing through the $\theta = 0$ point. The 110 regions on the emitting sphere which were the origin of the electrons hitting the screen at the measured positions were 60° apart. Now Eq. (8), which is the basis for our calculation of the areal magnification, predicts a value of y of 0.386 (a) for $\theta = 30°$. In this TEM, a = 0.90 cm, so that y = 0.348 cm. Thus, the predicted separation of the 110 spots on the screen, using the zero inertia approximation, is 2y = 0.696 cm. The observed separation is 0.842 cm, which is 121 per cent of 0.696 cm. Thus, an additional factor of 1.21 should be inserted into Eq. (8) to make the theory agree with reality. Thus, in this case a correction factor of $(1.21)^2$ or 1.46 should be put into the expression for the areal magnification, Eq. (10).

In conclusion, let us calculate the areal magnification of the TEM for the case where the emitter electrons are considered to have infinite inertia; i.e., where the emitted electrons follow a straight line from the sphere to the screen along the extension of a sphere radius. The magnification derived in this way will set an upper limit on the possible magnification of the TEM.

In this case, the form of y* is very simple

$$y^* = a \tan\theta^* \quad . \tag{11}$$

Thus

$$\frac{dy}{d\theta} = a \sec^2\theta \tag{12}$$

and

$$y \frac{dy}{d\theta} = a^2 \sin\theta \sec^3\theta \tag{13}$$

so that on substitution in Eq. (1) we find the magnification M_∞ as a function of θ for electrons with infinite inertia is

$$M_\infty = \frac{a^2}{r_0^2} \frac{1}{\cos^3\theta} \quad . \tag{14}$$

This is plotted in Fig. 8 along with the zero inertia magnification M. The actual magnification at a given θ will be somewhere between the limits established by these two curves, and in practice will fall closer to the lower curve.

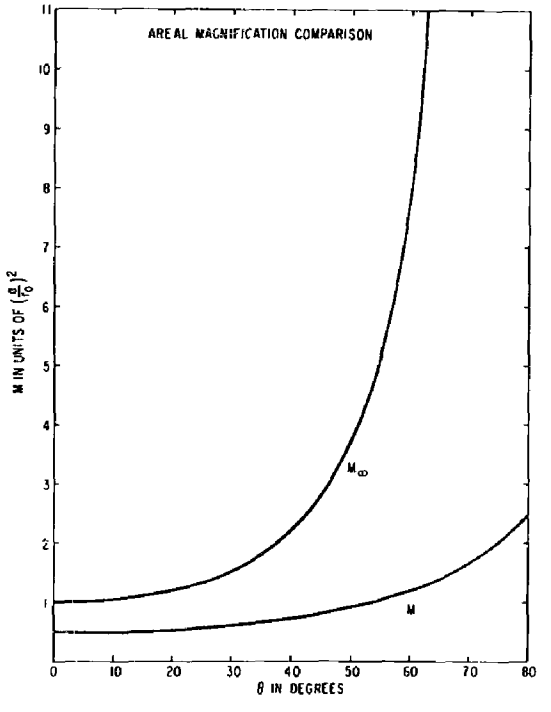

Fig. 8 Magnification as a function of initial emission direction.

D. Effects of Space Charge and Thermal Velocities of the Emitted Electrons and Ions

The choice of the voltage applied between the cathode and anode of the microscope was influenced by the effects of space charge and thermal velocities. If the voltage applied was too small, space charge would set a maximum current density which would be obtained from the surface of the ball. In the case of non-uniform emission from the ball which, in fact, was usually obtained, the space-charge spreading of the current bundles from the high emission regions would

make difficult the calculation of the emission current density at the ball surface from the measured value at the pinhole. A calculation of space-charge effects was thus desirable to establish what cathode-anode voltage would need to be applied to avoid these space-charge problems.

If the emission from the sphere was uniform, the concentric sphere solution of Langmuir and Blodgett[13] could be used to estimate the maximum current density obtainable without reaching the space-charge limit. This has been done and the results are presented for some typical ball and screen geometries which were used in these experiments. The emitting balls were all spherical and ranged in size from about 0.1 to 0.5 cm in diameter. None of the anodes were spherical and thus the concentric sphere solution could not be applied exactly. The space-charge effects, however, were important only in the near neighborhood of the emitting sphere and here the limiting current is relatively insensitive to the size and shape of the anode. Figure 9 presents the space-charge-limited current density of both electrons and cesium ions that can be drawn with various voltages applied between a 0.1-cm-diameter sphere and two different sizes of collecting spheres. Since current densities of 10^{-2} amp/cm^2 of either electrons or ions were the maximum ever encountered in these experiments, applied voltages of about 20 volts were sufficient to avoid space-charge limitations for electrons. The problem was more severe with the cesium ions, and very low voltage measurements would be impossible because of ion space charge.

The magnitude of the space-charge spreading of current bundles from small strongly emitting spots on the sphere is more difficult to estimate. The universal beam spread curve[14] was used to estimate the current density above which the space-charge beam divergence would exceed the geometrical beam divergence in the diverging electric field. This, of course, is a more severe limitation than is encountered in the microscope because the universal beam spread curve was derived for charges moving forward at constant speed. In the microscope geometry, the electrons are being accelerated and the current bundle thins out. Again space charge is only important near the emitting ball. It was found that the space-charge-limited currents in Fig. 9 were smaller than those estimated in this beam spread calculation and thus one is safe in using the values shown in Fig. 9 in determining the microscope voltage.

Another effect which must be taken into account in picking the microscope voltage is the effect of thermal velocities. The small initial velocity of the electrons or ions normal to the sphere surface is of no importance in the usual operation of this microscope. The tangential component, however, may contribute appreciably to the spreading of a current bundle from a strongly emitting spot if the applied voltage is low. Figure 10 shows the angular divergence of an electron path due to this effect as a function of applied voltage for various thermal velocities. This result was derived for motion between concentric spheres[15] but it is a good approximation for electron paths near the axis of the microscope where most of the measurements were made. Since the thermal velocities were generally less than 0.1 volt, applied voltages greater than 100 volts are sufficient to make this spreading small compared to the typical 5° geometrical spreading of an emitting region.

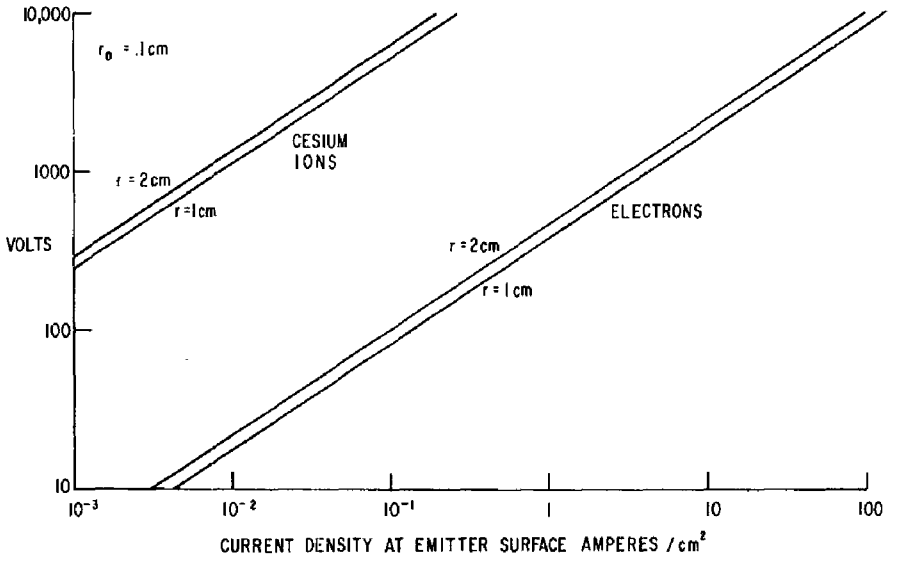

Fig. 9 Voltage limits for overcoming space charge for ion and electron currents.

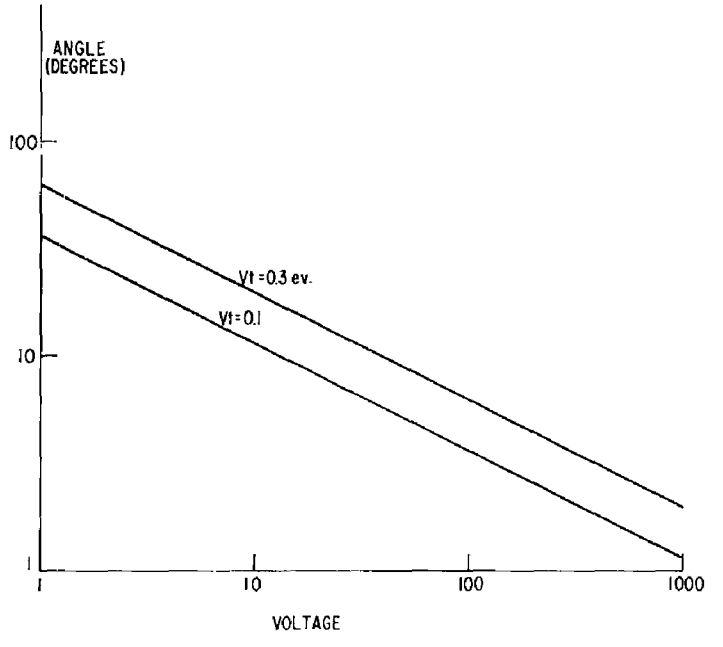

Fig. 10 Angle of spread of electron paths due to transverse velocities in a spherical diode.

Use of microscope voltages above 100 volts eliminated those effects which would make calculation of the magnification factor difficult. However, one often would like to know the value of thermionic emission densities with very low applied fields, and it is clear from the foregoing that these cannot be measured directly. In order to estimate this low field current, extrapolation of the high field currents by a Schottky plot has been used.

E. Temperature Calibration of the Emitting Spheres

The temperature of the emitting spheres has been determined when possible by use of a micro-optical pyrometer which was calibrated against a standard lamp. This instrument was also used to determine the variation in temperature of the sphere and supporting shaft. An average value of the spectral emissivity was used for each material, as the variation with crystal face was unknown. The very small variations in brightness temperature measured over a single-crystal sphere suggests that the variation with crystal face was quite small. It was suspected, however, that this might not be so for faceted or pitted surfaces.

Since alkali-metal coated surfaces emit significant current density at temperatures well below those measurable by optical pyrometry, methods of extending the temperature calibration were necessary. As described in the earlier publication,[8] infrared photography was used for part of this region. A method of extrapolation of the pyrometer measurements by use of the resistance of the emitter heater was suggested by J. M. Houston, and this has been used for most of these experiments. This extrapolation was based on the observation that a plot of log of the heater resistance vs emitter temperature was almost a straight line from room temperature through the optical pyrometer range. Since the heater resistance was measurable throughout this range, the emitter temperature was easily determined. A plot of this type is shown in Fig. 11. Once this graph was in hand, a plot of emitter temperature vs heater current (Fig. 12) could be prepared and this has been used for most of the samples.

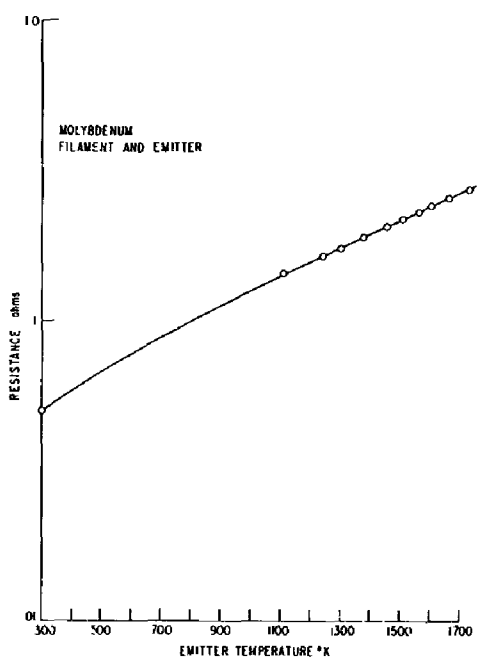

Fig. 11 Heater resistance vs emitter temperature.

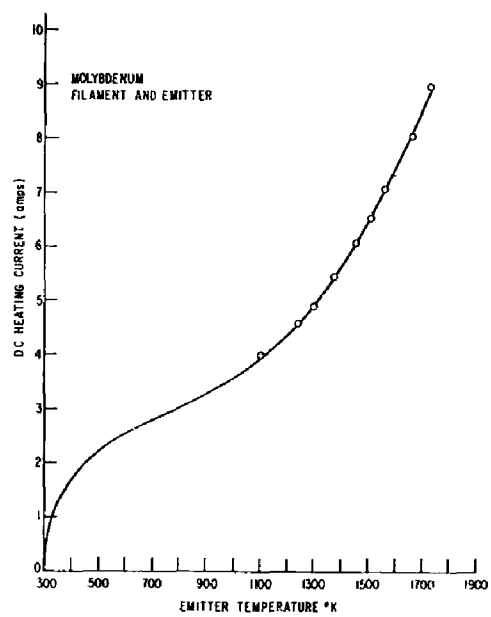

Fig. 12 Emitter temperature vs heater current.

III. EXPERIMENTAL RESULTS

Emission microscope experiments were done with balls of tungsten, tantalum, molybdenum, niobium, nickel, silver, rhenium, and niobium carbide in vapors of cesium, rubidium, or potassium. Some of the information obtained was qualitative and the other was quantitative. The first few tubes that were constructed did not permit the emission current density from individual crystal faces to be measured. Instead, only the total current from the emitting sphere and supporting shaft could be measured and the crystal faces which emitted most strongly could be determined from the patterns seen on the phosphor screen. With each succeeding tube, however, various improvements were incorporated. Figure 1 shows the version that was used most recently.

A. Body-centered Cubic Materials

All of the information on the body-centered cubic materials will be presented first. Quantitative data were obtained for tungsten, tantalum and molybdenum, but only qualitative information is available for niobium. Two tungsten crystals were operated in cesium vapor, and the tantalum bicrystal was studied in cesium and rubidium vapors. Two molybdenum samples were investigated in cesium and potassium vapors, while a niobium sample was measured in cesium vapor. All of these b. c. c. material samples initially had identical emission patterns when operated in cesium vapor. Differences, however, did develop later in the series of measurements probably due to the effects of contaminants.

1. Tungsten

(a) Emission Characteristics. The most extensive series of measurements were made with tungsten. These included measurements of current densities from various crystal faces, effects of contaminants on emission, electric field effects, and measurements of degree of coverage of various crystal faces by cesium in the 0.08 monolayer or less range.

When the tungsten emitter tube was first operated, the emission pattern observed had bright spots from the 110 region and weak emission from all other areas. After the tungsten emitter had been running for several hours, however, bright spots were also observed from the 112 regions. The emission from the 110 regions changed only slightly while the 112 spots were appearing. Most of the data which will now be presented were obtained after the 112 spots had appeared and is probably characteristic of contaminated tungsten. The contaminant effects seem to be very selective, however, and currents obtained from faces other than the 112 may not be much different from what would be obtained from cesium on clean tungsten.

Figure 13 shows a plot of electron and ion emission density for three different crystal faces of tungsten in cesium vapor vs reciprocal cathode temperature. Three different cesium reservoir temperatures have been used with the 100 surface. The electron emission from the 111 face is just about what would be expected from the 100 face, and this agrees with visual inspection of the pattern where these two faces have similar intensities. The 110 face, on the

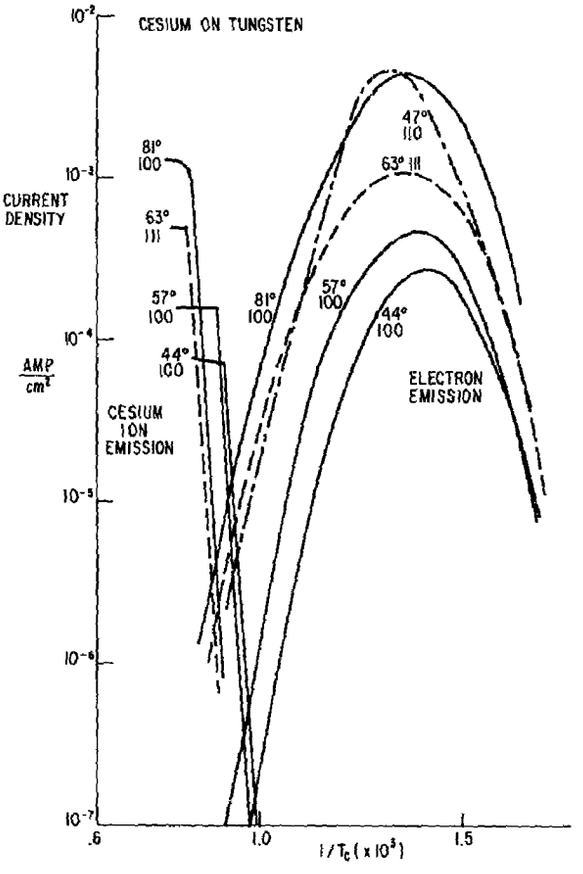

Fig. 13 Temperature dependence of ion and electron emission from tungsten planes.

other hand, at a cesium temperature of 47°C shows considerably more emission density than would be expected from either the 100 or 111 faces, at the same temperature. The ion emission curves for the 100 face, at different cesium temperatures, are in the order determined by the work functions of the emitting face. The ion emission curve for the 111 face appears displaced towards higher temperatures on the temparature axis, and the reason for this is unknown. All of these currents were measured with 300 volts accelerating the electrons and ions from the ball. The electron currents measured in this manner were slightly higher than would be measured at zero field as, for example, in Fig. 17.

Another experiment, done with a tungsten emitting ball, was directed toward answering a basic question about cesium-coated surfaces. The observed differences in emission density between crystal faces could be due to different coverages of the faces determined by preferential adsorption or could be due to different dipole moments of the cesium on the different crystal faces or a combination of these two effects. To check these possibilities the degree of cesium coverage of a strongly emitting 112 face and a weakly emitting 100 face was compared by flashing the ball and measuring the pulse of cesium ions which came off of each face using an oscilloscope. The ball was exposed to a constant flux of cesium atoms for the same time before each flash. This type of experiment can be done only when the surface coverage is less than 0.08 monolayer as discussed by Taylor and Langmuir.(16) This effect was nicely demonstrated in the following experiment.

The ball was exposed to a constant flux of cesium atoms for a fixed time and flashed and the ion pulse measured. The exposure and flash were repeated and the electron pulse measured. Next, the time of exposure to the cesium flux was increased and again the ion and electron pulses measured. It was found that the ion pulses reached a saturated value after about 4 minutes' exposure while the electron pulse was almost negligible after 4 minutes. It took about 15 minutes' exposure to the cesium flux for the electron pulse to reach a saturated value.

This may be explained as follows. Cesium readily leaves a heated surface as ions if the surface work function is higher than the ionization potential. The first partial layer of cesium deposited on the tungsten surface is sitting on a high work function surface. Additional cesium deposited on the initial layer, however, is sitting on a lower work function surface and thus when the ball is flashed the additional layers leave as atoms rather than as ions. It appears, then, that under the conditions of this experiment about 4 minutes is required to deposit this initial layer of about 0.08 monolayer, but this is insufficient coverage to give much electron emission. It is apparent, then, that to use the flashing technique to measure cesium coverage, the exposure times must be short enough that ion pulse height saturation has not set in and thus the total amount of cesium on the crystal face being investigated is removed as ions and measured in the ion current pulse.

The results obtained in these experiments are quite complex in their dependence on microscope voltage and degree of coverage. It is found, for example, that the emitted ion pulses usually show two main peaks with fine structure. Details of these experiments will be presented later. It may be stated now, however, that the ion pulses obtained from the crystal faces which are good electron emitters are usually larger than the ion pulses obtained from the poor electron emitting faces. Thus it appears that preferential adsorption must be at least part of the mechanism which accounts for the differences of electron emission between crystal faces.

(b) Anomalous Emission Patterns. In the course of our study of the emission from various crystalline faces of several single-crystal metal spheres in the presence of alkali-metal vapor, we sometimes observed intense emission from faces not ordinarily found to be copious emitters of electrons. These anomalous emission patterns were not present when the thermionic emission microscope was first used but appeared upon operating the tube for times which varied with the type of anomalous pattern. These unusual patterns were somewhat unstable in the sense that they could be temporarily removed or modified by suitable flashing or heat treatment of the emitter sphere. On the other hand, once an anomalous pattern had been observed in a tube it was impossible to return to the situation which obtained when the tube was new. In such a tube, the normal patterns would be persistently accompanied by some form of anomalous pattern. In general, the intensity of the emission in the anomalous portion of the pattern was higher than that of the normally emitting faces. Moreover, the current density of the emission from the "strange" faces reached a maximum at a somewhat higher temperature than did the current density of the emission from the "normal" faces.

The strangeness of these anomalous patterns and the high observed current densities associated with the anomalous emission make them of considerable interest. The greatest variety of anomalous patterns was observed in a thermionic emission microscope having a tungsten single-crystal emitter operating in cesium vapor, and we shall briefly describe the characteristics of the strange patterns found in this tube.

Upon first operating this W-Cs tube only normal emission patterns were obtained. However, after a few hours of operation of the thermionic emission microscope, emission from 112 regions was observed as well-defined spots on the screen. An example of this 112-spot emission is shown in Fig. 14(a). (The cesium pressure for this and the associated patterns is 1×10^{-6} torr.) The brightest spots in this picture correspond to emission from 110 regions on the emitter and are normally the only emitting face at this emitter temperature (479°C). In this picture somewhat less intense spots can be seen between the 110 spots. The anomalous spots correspond to emission from the 112 regions of the emitter.

At somewhat higher emitter temperatures the emission current density of the 112 emission surpasses that of the 110 emission, as can be seen in Fig. Fig. 14(b). Here, the emitter temperature has been raised to 551°C and the

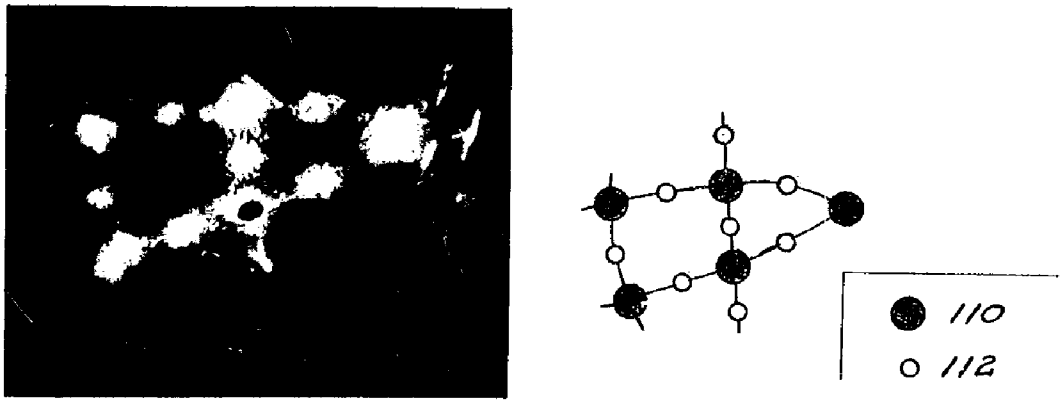

(a) 110 with 112 spot emission.

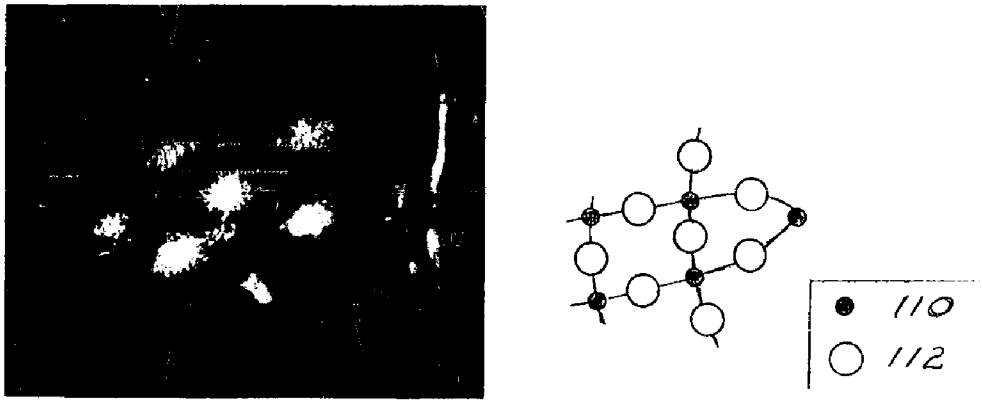

(b) 112 spot emission.

Fig. 14 Anomalous emission patterns of a Cs-W emitter.

(c) 110 with 112 ring emission.

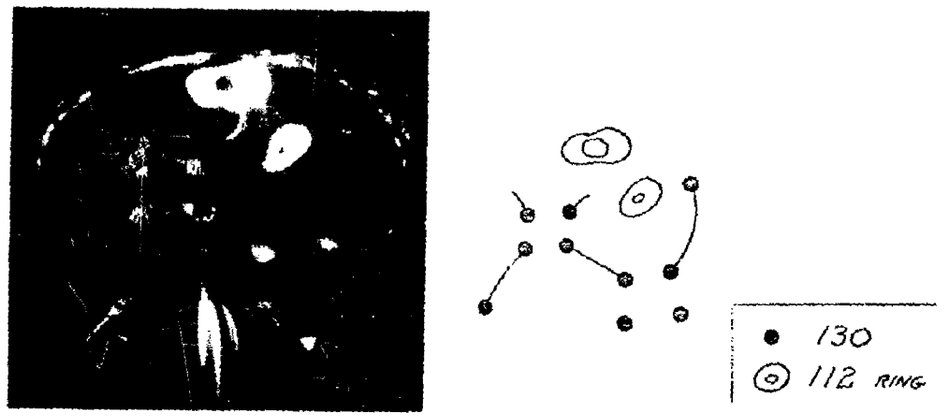

(d) 130 with 112 ring emission.

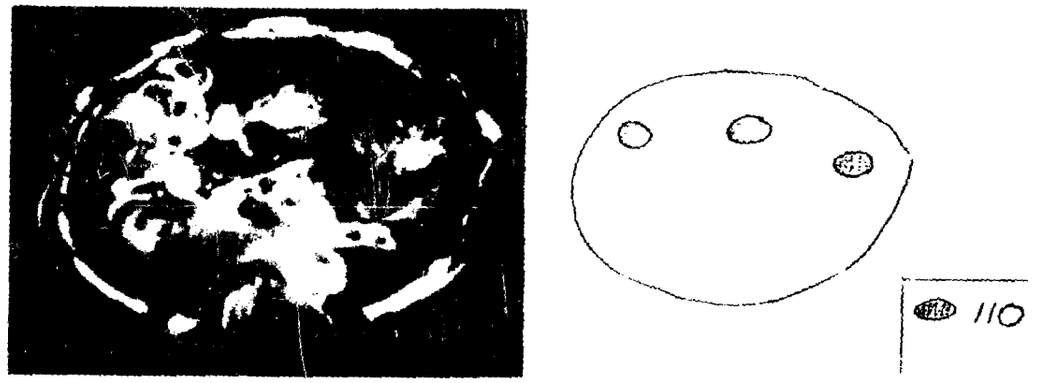

(e) 112 ring emission following heating above 700 °C.

Fig. 14 (continued).

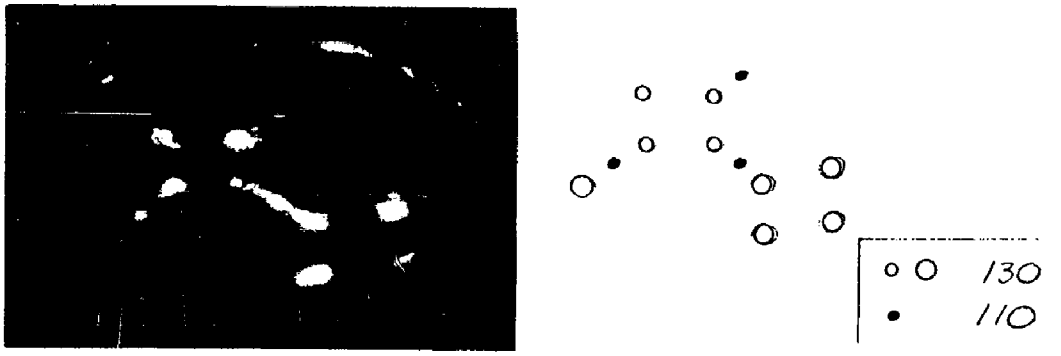

(f) 110 with 130 spot emission.

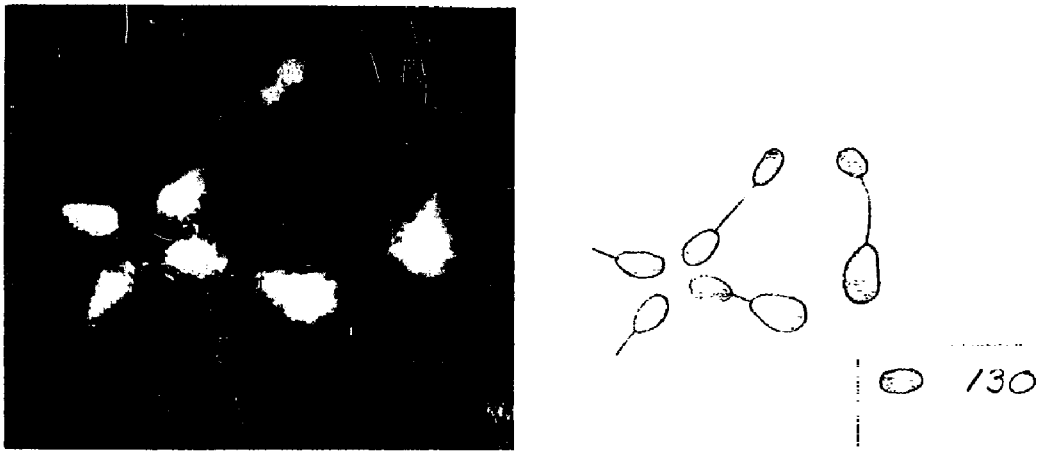

(g) 130 spot emission.

Fig. 14 (continued).

110 spots have become very dim. The 112 spots, however, are still quite bright. Apparently, the cesium atoms are now bound more tightly on the 112 faces than on the 110 faces, thus allowing emission to be observed at higher emitter temperatures from the 112 face than from the 110 face.

We attempted without success to eliminate the 112-spot emission by flashing the emitter for 1 minute at temperatures as high as 2700°K. The persistence of this pattern suggests that it is due to an adsorbed entity (in addition to cesium) which is so tightly bound to the tungsten that it is not removed at 2700 °K or which is present in such large quantities in the tube that it completely covers the 112 faces before an appreciable amount of cesium is adsorbed while the emitter is cooling down after the flash.

We speculate that this impurity adsorbant is fluorine and/or chlorine. It has been found by Metlay and Kimball[17] that fluorine is so tightly bound to clean tungsten that the last monolayer cannot be removed at 2600°K. Also, J. R. Young of this Laboratory has found that fluorine (along with chlorine) is given off in fairly large quantities by FN glass vacuum envelopes during electron bombardment of the glass. Such bombardment is almost inevitable in the operation of the thermionic emission microscopes. The slow buildup of the anomalous 112-spot emission might conceivably result from the production of fluorine and/or chlorine in this manner. It should also be noted that the pre-adsorption of fluorine has been found[18] to greatly enhance the emission from cesiated tungsten and molybdenum polycrystals. If fluorine were preferentially adsorbed on the 112 faces of our tungsten emitter, it would permit retention of the cesium and thus substantial emission at much higher temperatures than would be observed from an unfluorinated 112 face.

The spherical emitters as grown are usually mirror smooth as illustrated in Fig. 4. Figure 15(a) gives additional evidence on the condition of the surface of the newly formed sphere. This is an electron microscope picture of a replica of the surface of a tantalum sphere with a magnification of 30,000X. The only detectable structures seen on this sphere were grain boundaries, one of which passes through the center of the photo. The slight graininess results from the replication process.

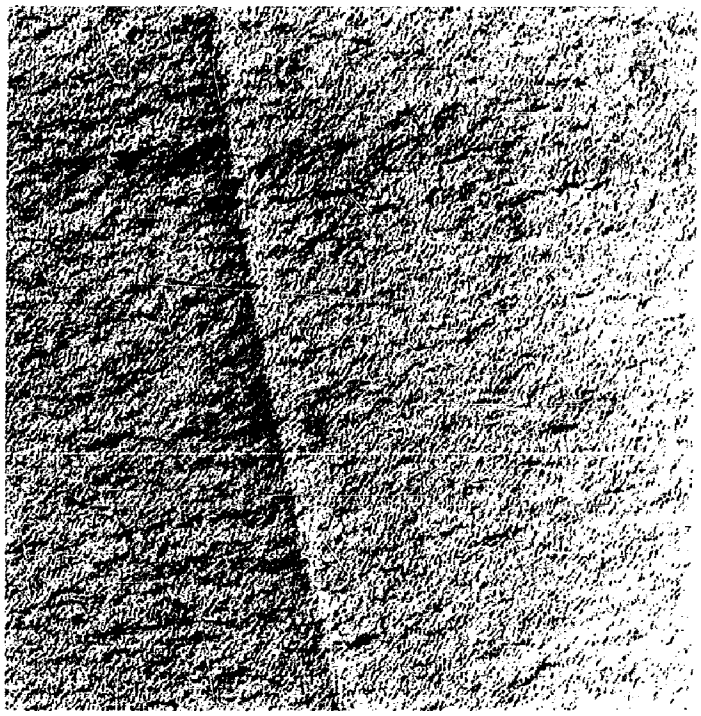

Fig 15(a) Electron microscope photograph of surface of tantalum sphere as produced by hanging-drop method. 30,000X

Fig. 15(b) Photomicrograph of surface of tungsten sphere after use in emission microscope. 250X

Quite in contrast to this, Fig. 15(b) shows the surface of a tungsten sphere which operated in an emission microscope for several months. This is an optical microscope photo of the side of the sphere facing the screen with a magnification of 250X, and severe attack of the surface is very evident. The area in focus is a circle of about 0.2 mm diameter, which is about one-fifth of the emitter diameter. If the random attack of the tungsten was of chemical origin, it may well have come from fluorine present in the tube. Fluorine is known for its ability to react with tungsten at low temperatures.(19)

A second type of anomalous emission pattern which was observed in the W-Cs tube is the 112-ring emission shown in Fig. 14(c) (along with the normal 110 emission). This "strange" pattern consisted of bright rings which sometimes appeared in the 112 regions. The emission associated with these rings is very intense, the maximum emission current density being about two orders of magnitude higher than any of the other observed patterns. The most interesting feature of this ring emission is that at all temperatures, in the range of interest, the emission current density of the ring emission is higher than that from any other face, including the other anomalous patterns. This implies that the minimum effective work function of the surface responsible for the ring emission is lower than that of any of the other crystal faces. The high intensity of the ring 112 emission is exhibited in Fig. 14(d) which shows the rings coexisting with a 130 pattern (to be described below).

The ring 112 pattern has the feature that above emitter temperatures of about 700°C, the pattern becomes quite mobile. Some striking configurations result, as shown in Fig. 14(e). Upon heating the emitter to 1100°C, the ring 112 pattern begins to transform to the spot 112 pattern, and at 1250°C the 112-spot pattern begins to transform to the 130-spot pattern and all traces of the 112-ring pattern have disappeared. The ring 112 pattern did not then reappear for a period of several days. It is interesting to note that the temperature at which the pattern becomes mobile is close to the melting point (684°C) of bulk CsF and the temperature at which the pattern disappears is close to the boiling point (1250°C) of bulk CsF. The shape of the ring pattern, the fact that the emission roughly follows a Fowler-Nordheim curve at intermediate field strengths, and the required growing time all suggest that this 112-ring emission may be due to field-enhanced thermionic emission from small CsF needles which have grown on the tungsten emitter. Further work is necessary, however, to verify this speculation.

The third and most interesting type of anomalous emission pattern observed in the W-Cs thermionic emission microscope is the 130 pattern which is shown in Fig. 14(f) along with vestiges of the 110 pattern. The 130 pattern is also visible in Fig. 14(d), and a more detailed picture of the 130 pattern is shown in Fig. 14(g). This 130 emission is perhaps the most unusual of the anomalous patterns in that the 130 face has not been found to be a particularly good emitter in earlier thermionic emission or field emission studies of tungsten in cesium vapor or other similar systems. Again this strange emission is of interest because it has a higher maximum emission current density than does the 110 emission and it peaks at a higher temperature than the 110 emission.

We have measured the zero-field emission current density in one of the center 130 spots and have compared it to the emission in an adjoining 110 spot. The zero-field data are obtained by making a Schottky plot at each emitter temperature and extrapolating the linear portion of the Schottky curve to zero field. A typical Schottky plot is shown in Fig. 16, this example being for the 110 emission at an emitter temperature of 444°C. In Fig. 17 are given the zero-field emission data for both a 130 and a 110 face. The 130-emission peak is higher by a factor of two than the 110 peak. Also, the 130 emission peaks at a higher temperature than does the 110 emission, the 130 peak lying at about 450°C and the 110 peak being close to 400°C. On the high-temperature side of the emission peak the 130-emission current density is about an order of magnitude higher than the 110 emission. Both the 110 and the 130 current density maxima lie above the comparable Langmuir-Taylor curve.(16)

The origin of this 130 emission is even more obscure than the other types of anomalous patterns. After flashing the tungsten emitter for 1 minute to temperatures above 2200°K the 130 emission is no longer observed although the 112-spot emission is present. If then the emitter is maintained in the temperature range of 1600° to 1800°K for a few minutes the 130 spots slowly reappear and the 112 emission decreases slightly. This "aging" process is reminiscent of the aging, at the same temperatures, found by Langmiur and Villars.(20)

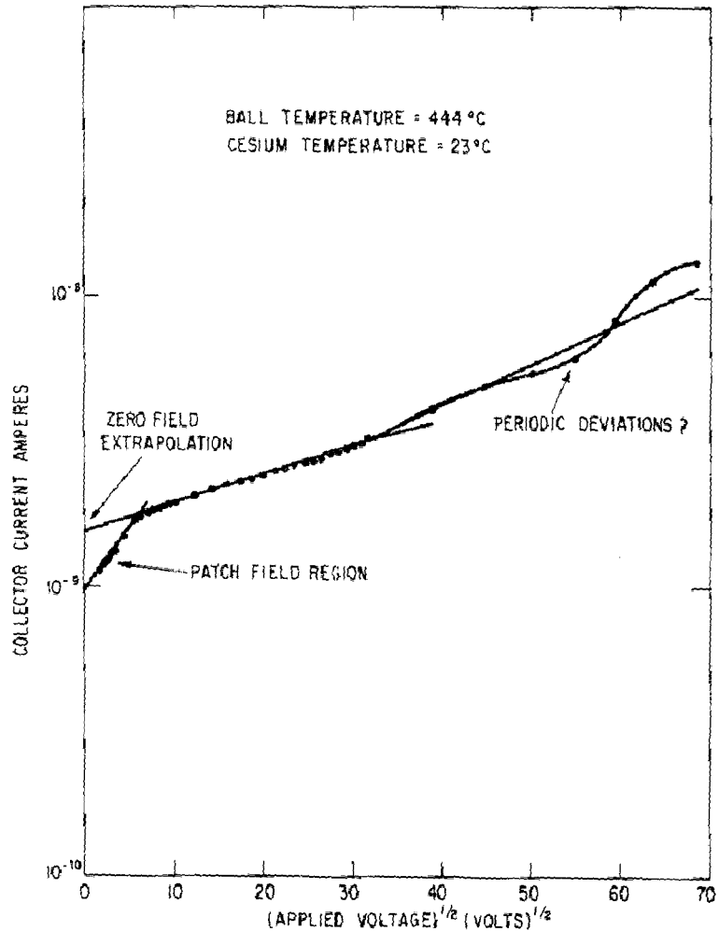

Fig. 16 Typical Schottky plot for 110 face of tungsten in cesium.

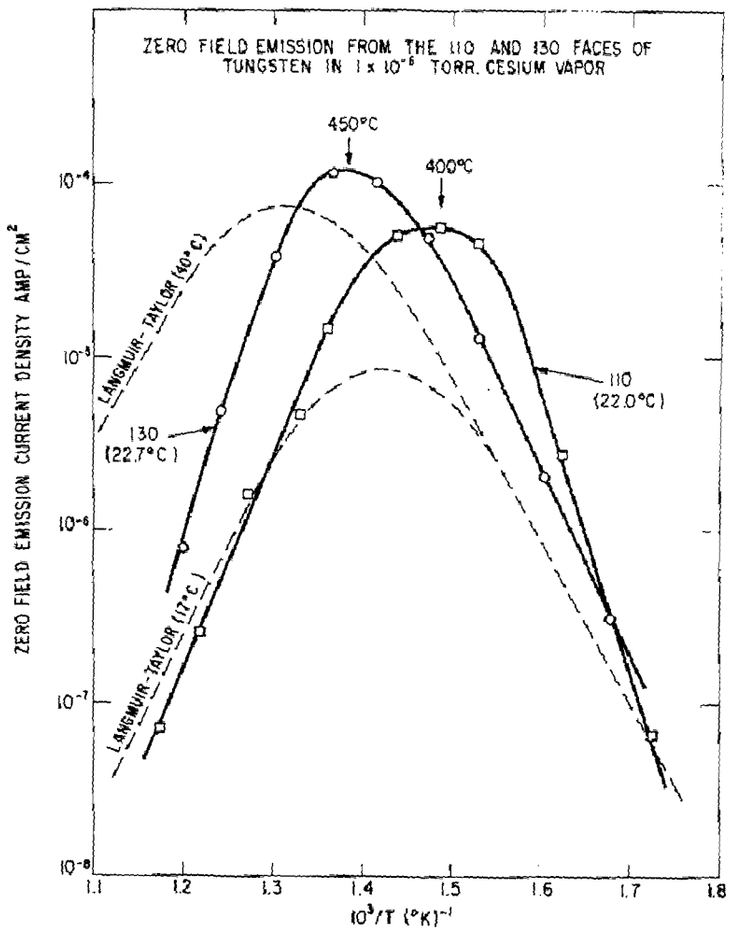

Fig. 17 Zero field emission from 110 and 130 faces of tungsten in cesium.

They found such aging necessary to activate their cesium-oxygen-tungstem emitters. Conceivably, oxygen present in the tube is selectively absorbed on the 130 faces. Oxygen is not as tightly bound on the tungsten surface as is fluorine and can be removed by a 2200°K flash for 1 minute.[20]

All of our speculations on the origin of the anomalous emission patterns are without firm experimental basis. We plan, however, to intentionally add fluorine, chlorine, and oxygen separately and together, to our W-Cs thermionic emission microscope tube and observe the resulting patterns. If these impurities are in fact responsible for the anomalous emission patterns we should be able to confirm these speculations about the nature of the surface layers which give rise to these strange emission patterns.

(c) Field Dependence of Emission. In the course of our emission measurements we have observed periodic deviations from the Schottky line which are in order of magnitude larger than those ordinarily observed for polycrystalline tungsten emitters. As can be seen from Fig. 16 periodic deviation amplitudes as large as 10 per cent of the Schottky line are observed, whereas polycrystalline tungsten emitters exhibit periodic deviation amplitudes of 0. 1 to 1 per cent.[21] Such large deviations, if real, may result from the fact that here we are looking at the emission of a single type of face of a single crystal. One would expect that in the emission from one face of a single crystal the interference between the electron waves quantum-mechanically reflected from various portions of the surface motive barrier would lead to periodic deviations[22] whose amplitude is characteristic of that face alone. In the case of polycrystalline emitters there is an averaging effect coming from the fact that several faces, all with different periodic deviation amplitudes and phases, are emitting at the same time, so that the net periodic deviation amplitude tends to be quite small. The large deviations which we observe here may also be in part due to the effect of the adsorbed cesium layer. The presence of the cesium will divide the motive barrier of the clean surface into two barriers, each of which will cause reflection. The width of these barriers will be less than in the case of the clean surface so that tunnelling currents can be larger.

We are undertaking a study of the periodic deviations from the Schottky line for the emission from several faces of our cesiated tungsten emitter in order (a) to determine whether our observed large amplitudes for the periodic deviations are indeed real, and (b) to use the periodic deviation data to determine the reflection coefficients for the various faces and to investigate the effect of the adsorbed cesium layer on the reflection coefficients. The occurrence of a high reflection coefficient for one or more of the faces might be indicative of the presence of effects of the bandstructure in the interior of the metal on the reflection coefficient predicted by MacColl[23] and discussed by Herring and Nichols.[24]

2. Molybdenum

The emission pattern for molybdenum initially showed high current densities from the 110 regions. After the tube had been operated for a few hours, strong emission was also obtained from the 112 areas. This is the same

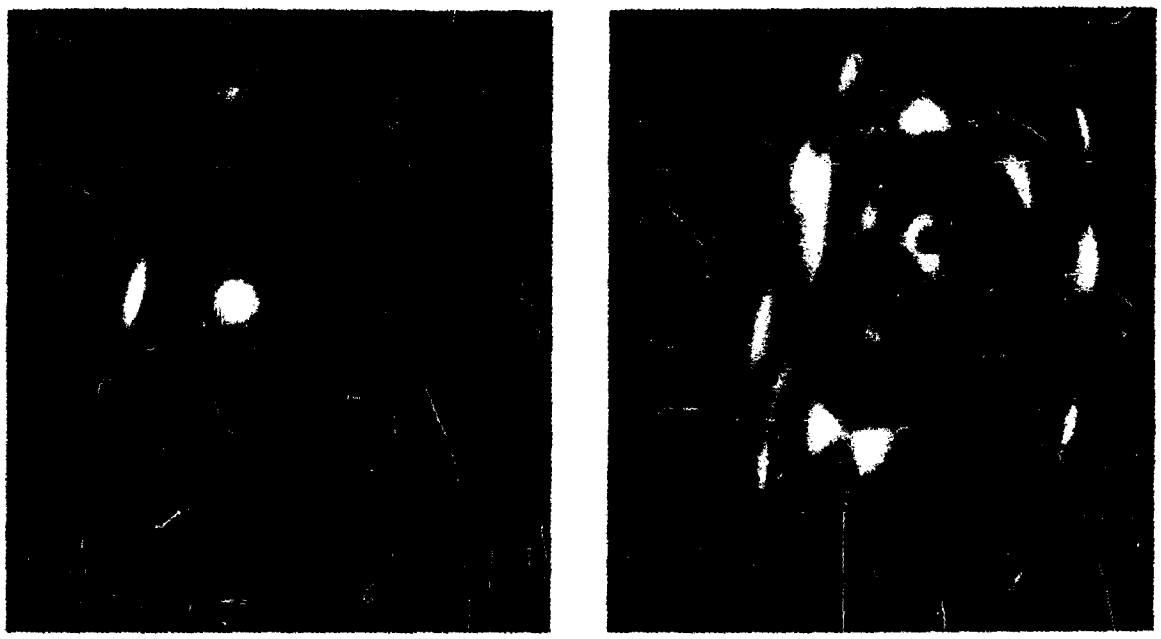

(a) (b)

Fig. 18 Emission from (a) clean and (b) contaminated molybdenum in cesium.

as was found for tungsten. Figures 18(a) and (b) show the initial pattern and the one obtained after the 112 spots have appeared. It was found that for about a day, intermittent flashing of the ball to a high temperature would remove the 112 spots and just leave the 110's. After that time, however, the 112 spots were present even after flashing. This behavior suggests that strong emission from the 112 spots is due to a contaminant gas which is slowly building up in the tube. After about a day the contaminant concentration has built up to such a level that the 112 areas are recoated before the ball has cooled down from the flash.

One may speculate as to the nature of this contaminant. In some mass spectrometer studies, as mentioned previously, J. R. Young has found that electron bombardment of the glass used in these microscope tubes produces persistent peaks of fluorine and chlorine. Some of the electrons from the microscope ball strike the glass walls and thus could build up a pressure of these gases after the tube has been in operation for a while.

Both fluorine and chlorine are small atoms which would fit in the rib structure of the 112 planes of molybdenum and tungsten and thus convert these planes into dense, close-packed planes with a high work function.

When the molybdenum emitter microscope was first operated the pinhole was set on a 112 spot. Thus it was possible to monitor the change in emission of both ions and electrons from this face as the contaminant content built up. Figure 19 shows the electron emission from the 112 face before and after contamination as well as emission from the 110 face. Figure 20 shows a detailed plot of the ion current from these two faces as a function of the current in the hairpin heater.

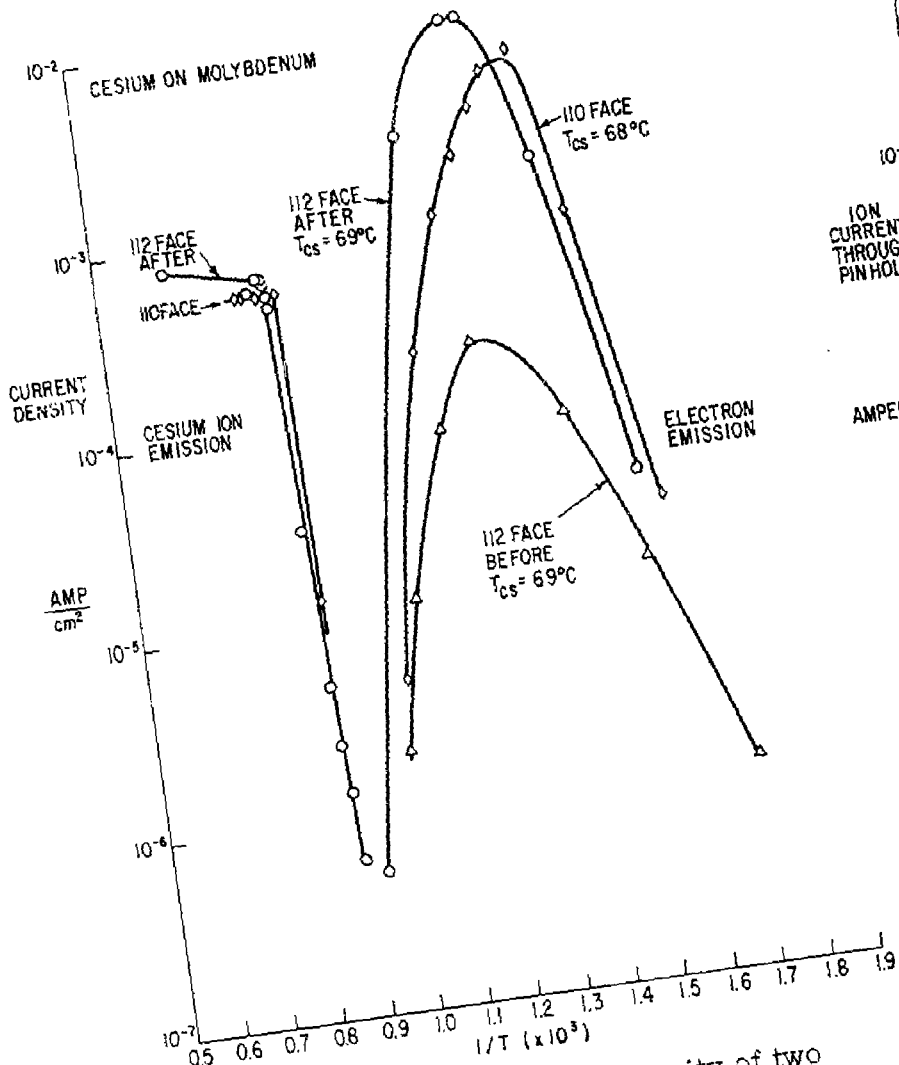

Fig. 19 Plot of emission current density of two planes of molybdenum in cesium.

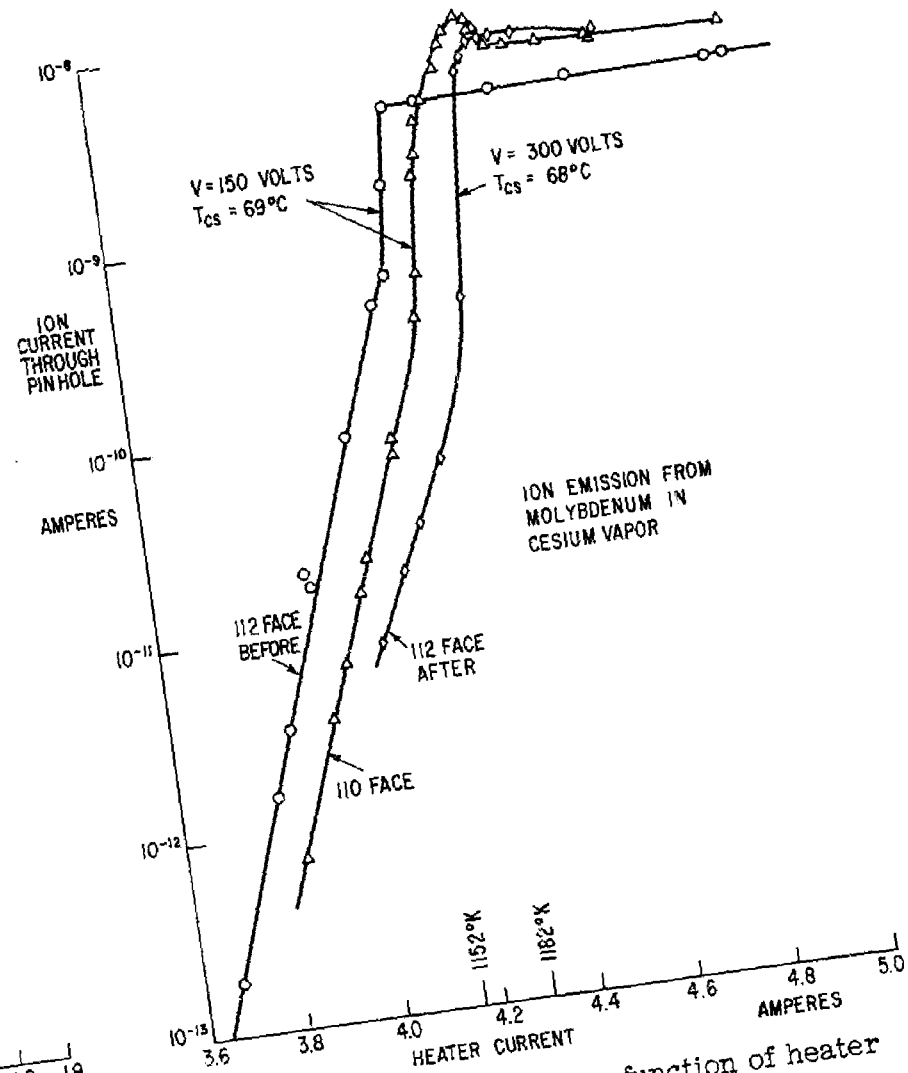

Fig. 20 Plot of ion current as a function of heater current for two planes of molybdenum.

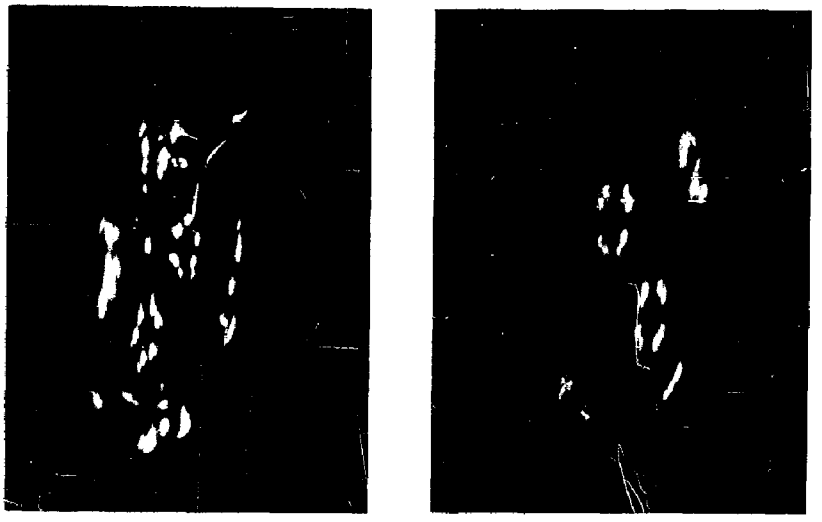

(a) (b)

Fig. 21 Emission patterns for molybdenum in potassium: (a) high temperature and (b) low temperature.

The molybdenum sample was also operated in potassium vapor and the emission patterns obtained were quite different from those obtained in cesium vapor. In potassium, it was not the closely packed atomic planes which yielded the strong emission but several of the high index planes. Figures 21(a) and (b) show the two patterns which were obtained when the molybdenum sphere was at a high and a low temperature.

3. Tantalum

Data obtained with tantalum have been presented in the earlier publication.(8) There are some interesting comparisons with tungsten and molybdenum which will be mentioned here.

The tantalum emitter was operated off and on for several months in cesium vapor, and throughout that time no change in the pattern was observed. The 110 regions were the only ones to yield strong emission which is quite in contrast to the results with tungsten and molybdenum. When tantalum was operated in rubidium the pattern consisted of 110 spots, but 100 regions also contributed at lower temperatures.

4. Niobium

The emission pattern obtained from niobium was the same as that from tantalum. The 110 spots were strong and no other areas contributed appreciably. One of the tubes constructed early in the course of these investigations contained niobium, tungsten, molybdenum, and rhenium emitting single-crystal spheres. It did not have the pinhole current collector, but each pattern could be seen on a phosphor screen and the total current from each ball could be measured. The

emission current densities obtained are uncertain because the exact area of the emitter which contributes current to the screen could only be estimated. The rhenium ball yielded the largest current density, with tungsten and molybdenum next and the niobium ball produced the least.

This tube containing the four emitters has recently been run again after 2 years to see how susceptible to contamination these four materials are. The present molybdenum pattern is almost homogeneous. The tungsten pattern also shows contamination but the 110 spots are still visible. The rhenium pattern has some new emitting regions but is not significantly changed, and the niobium pattern is identical to that obtained when the tube was new. Thus cesiated niobium appears to be a material which is a relatively poor emitter but which is almost immune to the effects of contaminants that arise in glass tubes.

B. Face-centered Cubic Materials

1. Nickel

Two samples of nickel have been operated in emission microscope tubes in cesium vapor in order to check the effects of surface preparation on emission patterns. The first single-crystal sphere was chemically etched in acetic and nitric acids and it was left with a faceted surface. The patterns obtained showed emission from the 111 region at high temperatures and from the 100 region at low temperatures. The spots in the pattern were quite diffuse and seem to have been made up of many smaller spots, a result which is not surprising in view of the roughness of the emitter surface.

The second sample that was electropolished in methanol and nitric acid was very smooth but it did have some etch pits. The pattern obtained with that sample still showed emission from the 111 region at high cathode temperatures and from the 100 region at low temperatures but nearby regions contributed at various temperatures such that the shapes of the 111 and 100 spots changed.

It may be either that the diffuseness of the patterns obtained with the chemically etched ball made the spot shape difficult to see or that the etching preferentially left 111 and 100 facets and removed other crystal planes.

2. Silver

An electropolished silver single-crystal sphere was operated with cesium vapor in the microscope but the pattern obtained was essentially uniform. The sphere was removed from the tube and found to have a matte surface which could be etched off in order to expose the single crystal material beneath. It was not rerun in the microscope, but some additional experiments were done which shed some light on this strange behavior of silver.

A tube was built in which a silver film could be evaporated on a window and the optical transmission of this film measured both before and after it was exposed to cesium vapor. It was suspected that there might be a reaction between the cesium and the silver producing a semiconductor, as has recently occurred with gold in cesium vapor.[25] The measurements of optical transmission done by Miss G. Lloyd of this Laboratory indicated that the silver film was somewhat

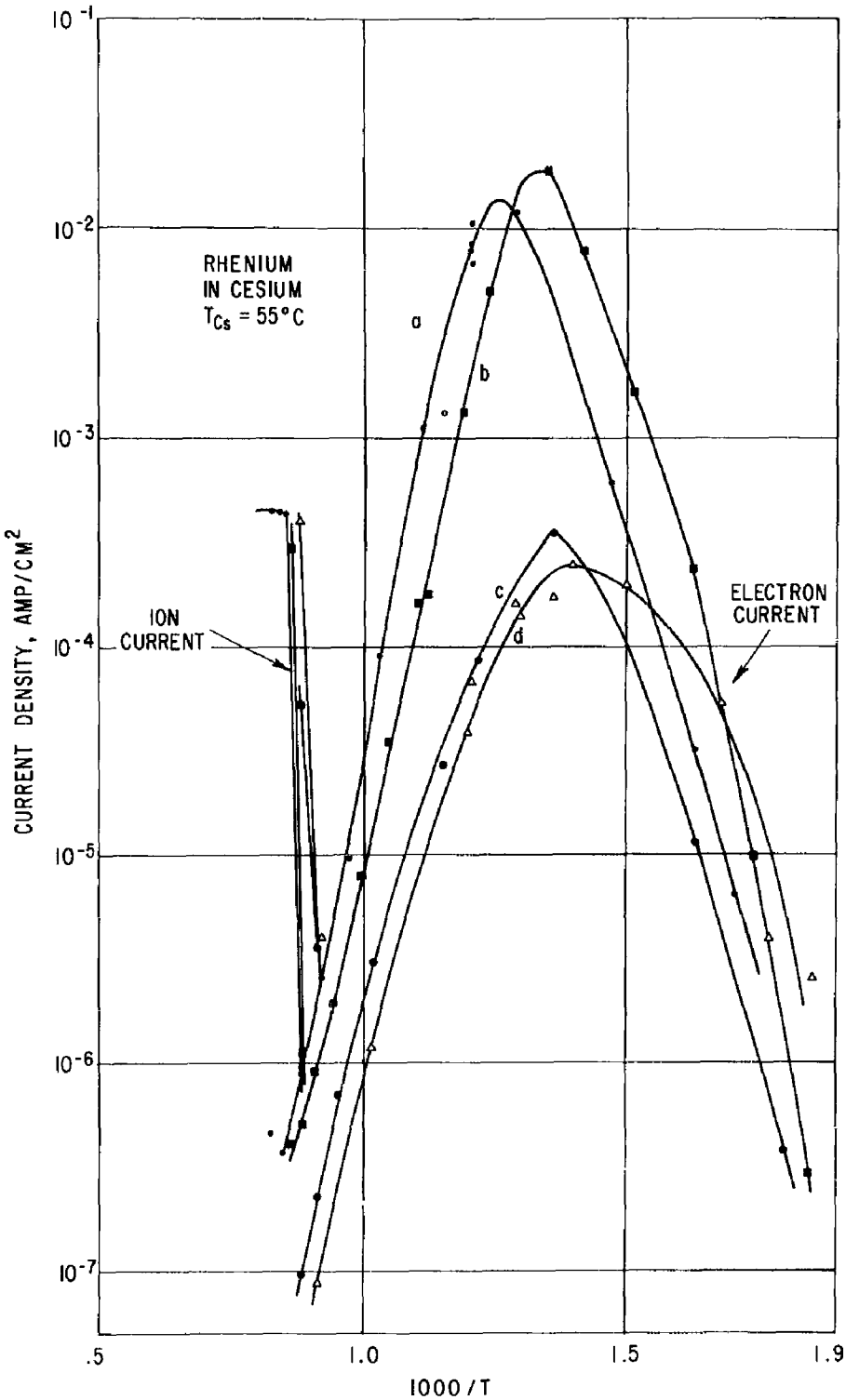

Fig. 22(a) Electron and ion emission density from four crystal faces of rhenium.

thinned by the cesium vapor but no change in shape of the adsorption characteristic could be detected. It was observed, however, that silver is soluble in liquid cesium. A single pass of a drop of liquid cesium over the film was sufficient to remove it.

It is possible then that the silver ball in the microscope tube may have been cool enough at some time to condense some liquid cesium which would explain its altered surface. Thus single-crystal silver surfaces do not appear promising for application in cesium diodes because of the ease with which their single-crystal surface is destroyed.

C. Hexagonal Materials

1. Rhenium

Electron and ion emission current densities have been measured for two strongly emitting and two weakly emitting crystal faces, and the results are presented in Fig. 22(a). The pattern obtained on the phosphor screen with this material is shown in Fig. 22(b). The center bright spots and the intermediate bright spots are associated with the 1010 and 1011 crystal faces. The two spots at the outer ring of the pattern which come from the 1000 faces were not measured. The dark regions measured were produced by the 1121 and 1231 faces. The ion current curves obtained are in the order determined by the surface work functions.

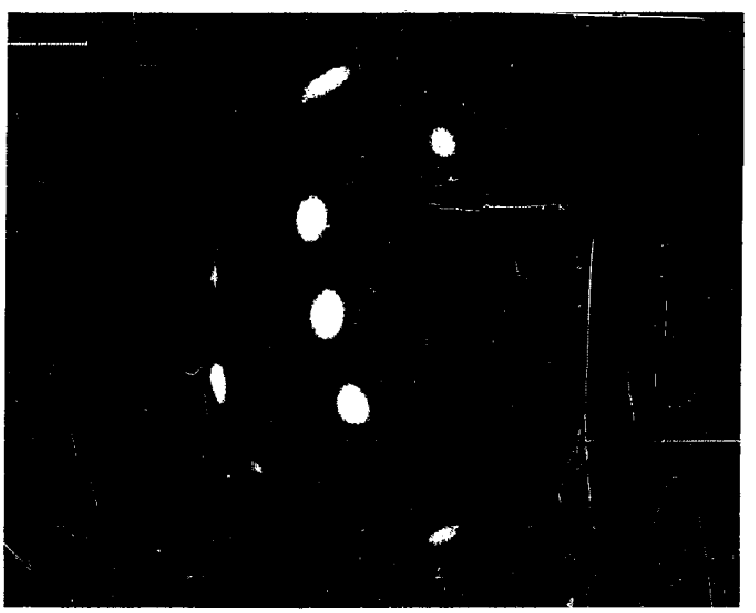

Fig. 22(b) Emission pattern for cesium on rhenium.

D. Cubic Materials

1. Niobium Carbide

This material has a sodium chloride type of lattice and the sphere used in these experiments was cut from a single-crystal block and electropolished. The sample was operated in cesium vapor and during the first run the tube developed a leak and went down to air. While the run was being made, however, the electron emission densities measured were quite high. The second tube using the same sample yielded the emission pattern shown in Fig. 23 and electron emission densities lower than those from tungsten. In order to learn if oxygen from the leak might have increased the electron emission and thus caused the difference between the first and second tests, the tube was rebuilt a third time with a silver tube to admit controlled amounts of pure oxygen. It was found, however, that oxygen left the emission pattern and the current density essentially unchanged.

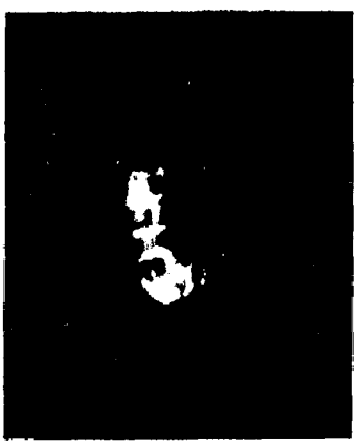

Fig. 23 Emission pattern for cesium on niobium carbide.

IV. DISCUSSION OF THE MICROSCOPE TECHNIQUE

This microscope offers several advantages over older techniques for emission measurement. Here we discuss some of these advantages along with the limitations. One of the advantages of this spherical thermionic emission microscope over the cylindrical forms first used by Johnson and Shockley, [2] and later used by Smith[26] and others is that the emission can be measured from all crystal faces instead of from just those lying on a line of the stereographic projection. For example, if the cylindrical crystal has a 110 orientation on its axis as frequently happens for b.c.c. materials, then only the crystal faces on the outer circle of Fig. 6 can be measured (i.e., the hhk planes).

Among the other advantages of the spherical microscope over the cylindrical is the relative ease with which the single-crystal spheres can be produced. As previously mentioned, they are easily produced from pure materials while growth of the long thin cylindrical filament crystals appears to be something of an art which often depends upon the controlled content of certain impurities in the wire. In addition, the sphere surface left from the molten state is usually mirror-like which is to be compared with the frequently strongly striated or faceted surface left by the heat treatment necessary to grow the cylindrical crystals. Another advantage of the spherical geometry over the cylindrical is the relative freedom of the spherical system from secondary electrons which reach the current collector aperture by indirect paths. [27]

In the cylindrical geometry, secondary electrons from any point on the anode cylinder can return to the current collector slot by a large number of paths. By contrast there is only one path from any point on the screen to the pinhole current collector in the spherical geometry. For most of the screen this path leaves the screen at an angle appreciably off of the normal. Secondary electrons from the glass side walls of the tube, however, can reach the pinhole with initial angles very near to the normal, but such secondaries can be avoided by arranging potentials such that the primary electrons do not strike the glass.

This microscope has not been used to measure the complete electron emission S curve because it was found that, when the cathode ball was heated hot enough to emit as a pure metal, the shield around the hairpin heater became hot enough to emit as a cesium-coated metal and spurious currents were obtained.

This type of microscope could also be used to measure the emission constants of pure metals but this has not been done yet because, when the ball is hot enough to emit without cesium, it is producing so much light that the emission pattern on a phosphor screen is masked. When this occurs, the crystal face that the pinhole is receiving current from is unknown. A way around this difficulty would be to operate the tube with cesium present and thus locate the pinhole in the pattern. The cesium could then be frozen out and the emission from the pure metal be measured.

When using such a microscope tube it is desirable to have as much of the tube as possible at the cesium bath temperature. While the equilibrium cesium pressure is determined by the coldest spot in the tube it often takes a surprisingly

long time for the equilibrium condition to be established, especially at low cesium pressures. For example, if the cesium pellet was broken and the whole tube left at room temperature, the cesium pressure should be in the range 1 to 2×10^{-6} torr. In theory, at this pressure every surface inside the tube should be coated with a cesium monolayer in a fraction of a second. Still it took from 2 to 3 days for equilibrium to be established. This is a significant effect that has been observed many times and the reason for it is not clear. It may be, however, that the cesium dissolves in or reacts with the tube parts especially the glass walls and all such processes must be complete before equilibrium can be established. When the cesium pressure is higher, of course, equilibrium is established much more quickly.

Whenever the emitting ball temperature was changed, the temperature of nearby parts such as the shield may also have changed. Thus, the cesium atom flux in which the ball was operating might not be in equilibrium with the tube walls. With each point taken for curves such as Figs. 13, 17, 18, it was necessary to wait until equilibrium was reestablished, and thus as a result taking quantitative data as a function of emitting ball temperature was a relatively slow process.

V. THE HIGH WORK FUNCTION PLANES OF METAL CRYSTALS

Since the high work function planes of metal crystals appear to be of particular importance for oxiated cathodes an effort was made to relate the value of the work function of these planes to the surface properties. A simple model was used for this calculation which gave some results in agreement with experiment. Probably the greatest usefulness of this model was in providing an intuitive picture of electron emission from various surface structures.

The model used was suggested by work of Bardeen[28] on the surface work function of sodium. He found that the largest contribution to the work function was due to polarization forces and the model used here assumes that the work function barrier is entirely the result of polarization forces. It is assumed that whenever an electron is in the neighborhood of a metal surface it polarizes each of the surface atoms which then in turn attract the electron. The resulting attractive force between the polarized atom and the electron is assumed to vary as $1/r^4$ and, when this is integrated over the surface atoms, the total force between the electron and the surface varies as the simple image force. This model has only been applied to densely packed atomic planes in which the second layer of atoms is well shielded by the first and thus the error of not summing over more than the surface layer of atoms may not be serious.

This calculation has been used to find the work necessary to remove an electron from the surface of the metal to an infinite distance for a variety of lattice sites for each of the close-packed planes of the body-centered and face-centered cubic lattices. It was found that the work necessary varies approximately as the square root of the surface density of atoms. This factor has been evaluated for the three most dense planes of these two lattices and the results are given in Table I. The metals with small lattice constants should provide the highest work function surfaces. One should remember, however, that the polarizability of the surface atom will appear in the constant of proportionality and this will be needed in comparing the work function of one metal with another. Unfortunately, little data of this sort appear to be available. The proportionality can be used, however, in comparing crystal faces of the same metal.

Another result obtained from this model is the suggestion that the rows of atoms that make up edges of close-packed atomic planes where a step to the next plane occurs may be unusually important in determining the electron emission from such regions. The model suggests that it would be easier for an electron to leave the region of such a step than to leave the surface of a close-packed plane.

As an example of the effect of these steps let us consider the 111 plane of the f.c.c. lattice and the region of the stereographic projection in the near neighborhood of that plane. The ideal 111 plane consists of atoms in close-packed triangular array with no atomic steps present. Other nearby planes such as the 233 consist of the same sort of close-packed planes but with a step drop to the next lower plane every 5 1/2 rows of atoms. Other planes even farther from the 111 are similar except that the steps occur more frequently. Not only does the number of steps per unit area vary but the structure of the row of atoms that makes up the step is also changed. Some of these rows have the atoms at the

TABLE I

Square root of the number of surface atoms per cm^2 (D) for the three densest planes of the body-centered and face-centered cubic lattices.

Body-centered Cubic Lattice

Face	$\sqrt{D}$	View of 100 Face
110	1.10/a	
100	1.00/a	
112	0.903/a	

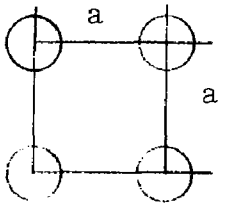

a = lattice constant in centimeters

Face-centered Cubic Lattice

Face	$\sqrt{D}$	View of 100 Face
111	1.52/b	
100	1.41/b	
110	1.19/b	

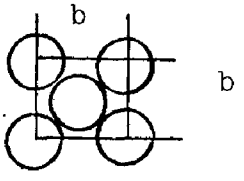

b = lattice constant in centimeters

shortest possible lattice spacing while others have the atoms arrayed with gaps between them. Figure 24 shows the atomic arrangement of the 110 face of a b.c.c. crystal and shows three of the different types of atom rows which can

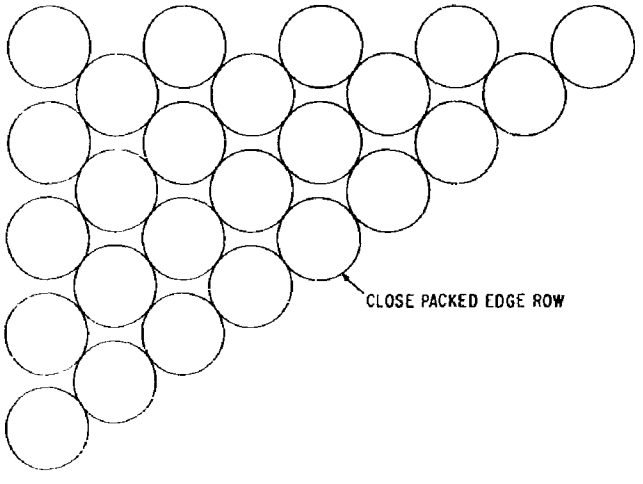

Fig. 24 Atomic arrangement along edges of 110 surface plane for b.c.c. lattice.

make up steps with this plane. The polarization model suggests that it is more difficult for an electron to leave the close-packed row than it is for an electron to leave the loose-packed ones.

It was found that certain crystal faces have close-packed rows and other ones have loose rows and that all of the faces which have close-packed rows lie along a few lines on the stereographic projection. These close-packed row lines have been plotted for the f.c.c. and b.c.c. lattices in Figs. 25 and 26.

The occurrence of these close-packed rows may explain the appearance of lines of low emission density which are seen in the field emission patterns of nickel,[15] iron,[15] copper,[15] iridium,[29] rhodium,[29] gold,[15] aluminum,[15] titanium,[15] vanadium,[15] tungsten,[15] tantalum,[30] and niobium.[31] All of

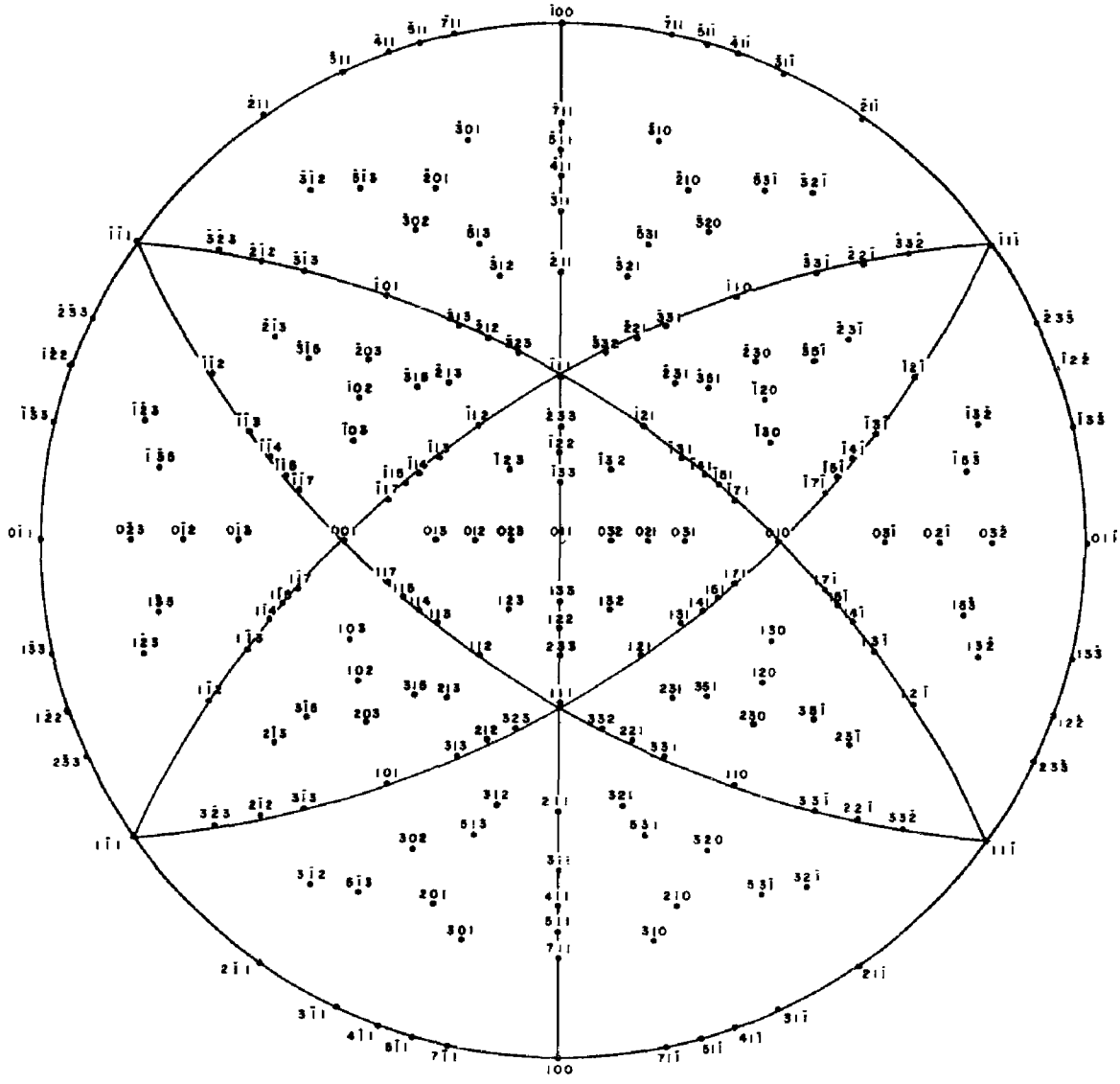

Fig. 25 Close-packed row lines on surface of f.c.c. lattice.

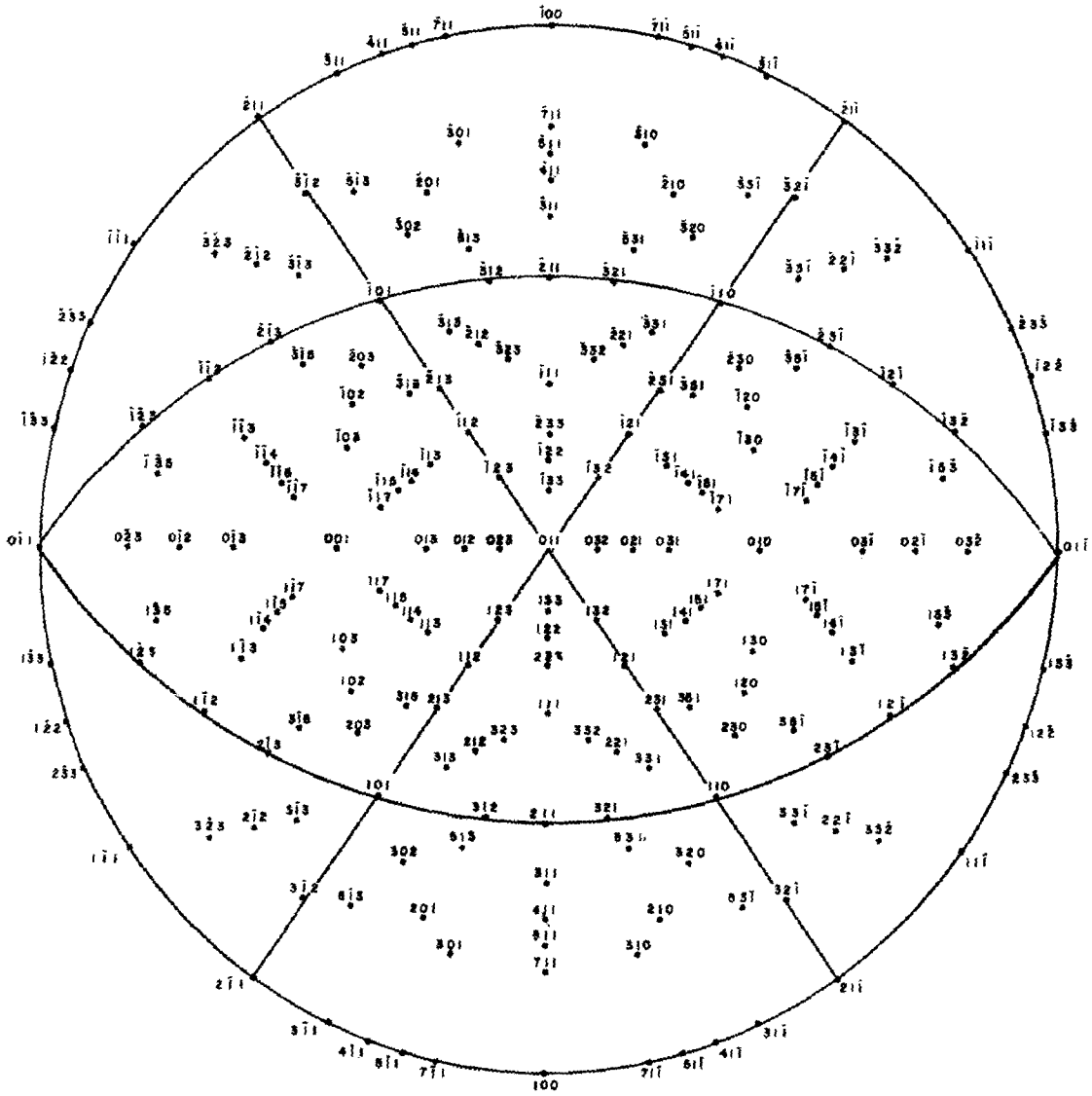

Fig. 26 Close-packed row lines on surface of b.c.c. lattice.

these materials show lines of low emission which are the same as the close-packed row lines shown in Figs. 25 and 26. The explanation may be as follows. Along these lines, both the crystal planes and the atom rows which make up the steps are close packed and low electron emission is obtained. Between these lines the crystal planes are still close packed but the atom rows are loose packed and thus it would appear that the larger electron density obtained is due mostly to the steps made up of the wider spaced atom rows.

VI. CONCLUSIONS

A. Emission from Alkali Layers on Clean Metals

There are a few generalizations that are suggested by these measurements and observations and these will now be discussed. The b.c.c. metals when covered with a fraction of a monolayer of cesium all showed the strongest emission at high cathode temperatures from the 110 plane which has the closest packing of surface atoms and the highest work function when clean. Similarly, the f.c.c. material, nickel, had strongest emission from the 111 plane which when clean had the highest work function, but it also had a lower temperature emission peak from the second densest crystal plane (i.e., the 100). Rhenium, a hexagonal material, had strong emission from the three high atomic density planes of that lattice. All of these highly emitting planes when cesiated, have work functions when clean which are considerably higher than the ionization potential of cesium, which is 3.89 volts. The emission from tantalum in rubidium was similar with the high-temperature emission being from the 110 face but with an additional peak at low temperatures from the 100 plane. The ionization potential of rubidium is 4.16 volts. In all these cases, however, the high-temperature emission patterns are remarkably simple, consisting only of small emitting areas at the center of the high work function areas with all other areas contributing much less emission density.

The results obtained with molybdenum in potassium vapor are quite in contrast to the above and both the high- and low-temperature patterns consist of emission from the atomically rough planes which would have low work function when clean. The ionization potential of potassium is 4.32 volts. Another complex pattern is obtained from niobium carbide operating in cesium. In this case, the work function of the niobium carbide is lower than that of most of the other materials studied.

It appears, then, that when the work function of the base metal plane is much higher than the ionization potential of the alkali vapor, the high-temperature pattern consists simply of emission from the high work function planes. On the other hand, when the ionization potential and work function are more nearly comparable, the patterns are complex and, in general, the high work function planes do not contribute strongly. These observations are nicely explained by the following model.

In general, the binding of cesium to a surface is dependent upon the nature of the surface binding sites. There is, however, a strongly overriding effect that occurs whenever the surface work function is higher than the alkali ionization potential and the surface temperature is high. Under these conditions the alkali atom is ionized and bound to the surface by image forces. The only time the nature of the surface binding sites becomes important is when conditions are less favorable for producing ions, namely, that the work function is low.

There are several other bits of evidence which support this picture.

1. In some other studies the emission patterns from metals coated with barium[5] (ionization potential 5.19 volts) have been observed and the patterns are complex with most emission from the rough planes and little from the smooth, high work function planes.

2. An attempt was made to match a surface lattice of cesium atoms to the surface lattice of the metal planes which show high emission density, the idea being that when a good match was obtained adsorption would be strong. While this model works for the 110 planes of tungsten and molybdenum, it does not appear to work without considerable lattice distortion for any of the other planes which strongly emit at high temperature. These planes have a great variety of binding sites with different symmetry properties and lattice constants and the only property they appear to have in common is a relatively high work function.

3. It is surprising that cesium should bind to the atomically smooth planes. One would expect that an adatom would be more strongly held at an atomic step or hollow in one of the rougher crystal planes. The binding by image forces on the smooth planes appears to be a way around this difficulty.

4. An additional bit of evidence that has come out of these studies is given by the low-temperature pattern of tantalum in cesium vapor [see Fig. 2(b), Ref. 8]. When the emitting ball is operated at high temperatures sharp 110 spots are obtained but at low temperatures these spread out until the largest emission is obtained from the region of the 321 planes and less emission is obtained from the 110. The weaker site dependent binding forces become important at low temperatures while the cesium layer on the 110 plane is thicker than the optimum.

The theoretical model of Rasor and Warner[32] is based on binding of cesium to the surface as ions. The results of this theory are in excellent agreement with the experimental measurements made in these studies for the high-temperature patterns where the surface coverage is less than a monolayer. One would expect, however, that this theory would be less accurate at lower emitter temperatures where the nature of binding sites is believed to be important.

B. Emission from Alkali Layers on Contaminated Metals

It would appear that contaminants added to metal surfaces can influence the electron emission in the presence of alkali metals in at least two ways: (1) the contaminants can change the work function of the metal surface and consequently change the binding of the alkali in the form of ions; (2) the contaminant can chemically bond with both the metal and the alkali metal.

The way that the contaminants work on cesiated tungsten and molybdenum is not known but, as has already been suggested, the 112 spots may be the result of an increase of the metal work function. Fluorine or chlorine could set down in the 112 rib, convert it into a high density plane, and then hold the cesium as ions. This is confirmed by field emission measurements which indicate that the 112 planes of tungsten and molybdenum are the second highest work function planes of those materials. This is a different interpretation than is usually given to this information by field emission workers who regard the high work function to be an inherent property of the 112 plane rather than being due to a contaminant. There is sufficient evidence from these measurements, however, to warrant re-examination of the work function of the 112 plane free of contaminants.

To review the evidence briefly: the cesiated emitters of tungsten, molybdenum, tantalum, and niobium initially all have the same emission pattern consisting only of 110 spots. After a few hours running, the 112 faces of tungsten and molybdenum begin emitting due to the arrival of contaminants. The field emission patterns of tungsten and molybdenum[31] have high work functions on the 110 and 112 faces. Niobium[31] and tantalum[30] show high work functions only for the 110 face. Thus the field emission patterns and contaminated thermionic patterns are in agreement.

It is known that fluorine and chlorine are liberated when electrons bombard the glass of these tubes. The thermionic microscopes used for the cesium studies had the potentials arranged such that most of the electrons struck the phosphor screen which was on a metal plate. Only a few stray electrons reached the glass walls. The accelerating voltage used in these tubes was between 100 and 300 volts.

On the other hand, both the field emission tubes and the cylindrical thermionic microscope tube of Nichols[33] have their screens on glass and thus the electrons bombard the glass directly. The voltage used in the field emission tubes is over 10 kilovolts and that used by Nichols was between 1000 and 3500 volts. It may be, then, that the production rate of the halides and its efficiency of return to the emitter is so high in the case of these high-voltage glass screen tubes that the emitter becomes contaminated within a very brief period after the voltage is applied.

Smoluchowski[34] has made a theoretical calculation of the work function of various crystal faces of tunsten. Using a smooth charge distribution he found the sequence of faces in the order of decreasing work function to be 110, 100, 112, and 111. This is in agreement with the result of the simple polarization model and the experimental measurements with cesium. Upon introducing a correction for a nonsmooth charge distribution the sequence becomes 110, 112, 100, and 111. It would be useful to repeat this calculation in light of recent knowledge that the anisotropy of the work function is much larger than it was previously believed to be. The results of Nichols upon which this calculation was based gave a difference of work function between the 110 and 111 faces of about 0.3 electron volt. More recent measurements yield a value of this difference in the range 1.2 to 1.6 electron volts.[27, 35]

It would also be of interest to carry out this calculation for either tantalum or niobium for which there is agreement that the sequence of face work functions are in the order 110, 100, 112, and 111.

ACKNOWLEDGMENTS

The authors would particularly like to acknowledge the assistance of T.A. Howlett, who skillfully carried out many of the measurements presented in this report. Many members of the Research Laboratory shops have carried out the construction and processing of the microscope tubes. The authors have benefited from discussions with J M. Houston, V.C. Wilson, M.D. Gibbons, and V.L. Stout. Our most sincere thanks to all of them.

APPENDIX

VALIDITY OF APPROXIMATIONS USED IN THE CALCULATION OF THE AREAL MAGNIFICATION OF THE THERMIONIC EMISSION MICROSCOPE

Let us consider the potential distribution of two point charges of equal but opposite charge of magnitude q separated by the distance 2b. We may consider these charges to be located on the x-axis of a cartesian coordinate system with the negative charge at -b and the positive charge at +b. We shall first show that the equipotential surfaces located close to the point charges are, to a good approximation, spheres whose centers are located close to the point charge. We shall then evaluate the deviations from sphericity and the displacement of the center of the equipotential "sphere" away from the position of the point charge in the case where the equipotential "sphere" around x = -b represents the emitter in our thermionic emission microscope.

Now, since the potential distribution of two point charges is axially symmetric about the line joining the charges, we may solve the equivalent two-dimensional problem. If y is the second cartesian coordinate, the potential V at an arbitrary point in the xy plane is given by

$$V = \frac{q}{4\pi\epsilon}\left\{\frac{1}{[(x-b)^2 + y^2]^{1/2}} - \frac{1}{[(x+b)^2 + y^2]^{1/2}}\right\} \qquad \text{(A1)}$$

in MKS units where ϵ is the capacitivity of free space. After shifting the origin of the coordinate system to x = -b and transforming to the polar coordinates, (r, θ), Eq. (A1) will become

$$\frac{4\pi\epsilon V}{q} = -\left\{\frac{1}{r} - \frac{1}{[r^2 - 4br\cos\theta + 4b^2]^{1/2}}\right\}$$

or

$$r = R\left\{1 - \frac{\frac{r}{2b}}{\left[1 - \frac{r}{b}\cos\theta + \frac{r^2}{4b^2}\right]^{1/2}}\right\} \qquad \text{(A2)}$$

where

$$R = -\frac{q}{4\pi\epsilon V} \quad .$$

Now, the radius of our emitter spheres, r_0, is always much less than the sphere-to-screen distance, so that we are in the realm where $r/b \ll 1$. Expanding the denominator of Eq. (A2) and keeping terms only to order $(r/b)^2$

$$r = R\left\{1 - \frac{r}{2b}\left[1 + \frac{r}{2b}\cos\theta\right]\right\}$$

or

$$r = R\left[1 - \frac{r}{2b}\right]\left[1 - \frac{\cos\theta\left(\frac{r^2}{4b^2}\right)}{\left(1 - \frac{r}{2b}\right)}\right]. \qquad (A3)$$

This equation is of the same form as the equation of a circle referred to a coordinate system whose origin is not at the center of the circle but displaced along the x-axis (in the +x direction) by Δ, where Δ is much smaller than the radius. To see this, let us consider the equation of such a circle in the cartesian coordinate system (u, v). This may be written as

$$(u + \Delta)^2 + v^2 = T^2 \qquad (A4)$$

where T is a given radius. Transforming to the polar coordinates, (s, ϕ), Eq. (A4) becomes

$$s^2 + 2s\Delta\cos\phi + \Delta^2 = T^2 \quad . \qquad (A5)$$

Solving for s, we have

$$s = T\left\{\left[1 - \frac{\Delta^2}{T^2}\sin^2\phi\right]^{1/2} - \frac{\Delta}{T}\cos\phi\right\} \quad . \qquad (A6)$$

Expanding the square root, under the condition that Δ is much smaller than the radius T

$$s = T\left[1 - \frac{\Delta}{T}\cos\phi - \frac{\Delta^2}{2T^2}\sin^2\phi + \ldots\right] \quad . \qquad (A7)$$

To first order in Δ/T, Eq. (A7) is

$$s = T\left[1 - \frac{\Delta}{T}\cos\phi\right] \qquad (A8)$$

which has exactly the same form as Eq. (A3). Thus, we may identify the quantities

$$T = R[1 - r/2b] \tag{A9}$$

$$\Lambda = R[r^2/4b^2] \quad . \tag{A10}$$

Therefore, to second order in (r/b) the equipotential surfaces close to the point charge are spherical. For a given value of (r/b) we may evaluate the displacement of the center of the equipotential from the point charge.

In the case of the thermionic emission microscopes, the equipotential sphere which coincides with the emitter has a radius, r_0, of about 1/15 of the sphere-to-screen distance. Thus, any deviation from sphericity will be of the order of $(r/b)^3$ or (1/3375) or less than 1 part in 10^3. The displacement of the center of the equipotential from the point charge will be from Eq. (A10)

$$\Delta = r_0 \left[\frac{1}{(4)\ (225)} \right] = \frac{r_0}{900} \quad ,$$

that is, about one-thousandth of the equipotential (emitter) radius. Both the deviation from sphericity of the equipotential and the displacement of its center from the position of the point charge are less than our experimental error in measuring these quantities.

REFERENCES

1. E. Bruche, Jahrb, Forschungsinst A.E.G., 4, 25 (1933-1935).
2. R.P. Johnson and W. Shockley, Phys. Rev., 49, 436 (1936).
3. S.T. Martin, Phys. Rev., 56, 947 (1939).
4. E.W. Müller, Z. Physik, 106, 541 (1937); Z. Physik, 108, 668 (1938).
5. R.J. Good, Jr. and E.W. Müller, "Field Emission," Handbuch der Physik, Vol. 21 (1956).
6. H.F. Webster, Bull. Am. Phys. Soc., (2), 5, 348 (1960).
7. H.F. Webster, Bull. Am. Phys. Soc., (2), 6, 343 (1961).
8. H.F. Webster, J. Appl. Phys., 32, 1802 (1961).
9. W.J. McG. Tegart, The Electrolytic and Chemical Polishing of Metals, Pergamon Press, Ltd. (1956).
10. L.A. Harris, Introduction to Electron Beam Technology, Robert Bakish, ed., John Wiley and Sons, Inc., New York (1962), Chap. 2.
11. W.R. Smythe, Static and Dynamic Electricity, 2nd ed., McGraw-Hill Book Co., Inc., New York (1950), p.9.
12. O. Klemperer, Electron Optics, 2nd ed., Cambridge Univ. Press, London (1953), p. 175.
13. I. Langmuir and K.B. Blodgett, Phys. Rev., 24, 49 (1924).
14. K.R. Spangenberg, Vacuum Tubes, McGraw-Hill Book Co., Inc., New York.
15. R. Gomer, Field Emission and Field Ionization, Harvard Univ. Press (1961).
16. J.B. Taylor and I. Langmuir, Phys. Rev., 44, 423 (1933).
17. M. Metlay and G.E. Kimball, J. Chem. Phys., 16, 779 (1948).
18. R.L. Aamodt, L.J. Brown, and B.D. Nichols, J. Appl. Phys., 33, 2080 (1962).
19. W.H. Kohl, Materials and Techniques for Electron Tubes, Reinhold Press, New York (1960), p. 263.
20. I. Langmuir and D.S. Villars, J. Am. Chem. Soc., 53, 486 (1931).
21. D.W. Juenker, J. Appl. Phys., 28, 1398 (1957).
22. E. Guth and C.J. Mullin, Phys. Rev., 59, 575 (1941).
23. L.A. MacColl, Bell System Tech. J., 30, 888 (1951).
24. C. Herring and M.H. Nichols, Revs. Modern Phys., 21, 185 (1949).
25. W.E. Spicer, Phys. Rev., 115, 57 (1959).
26. G.F. Smith, Phys. Rev., 94, 295 (1954).
27. J.M. Houston, thesis, MIT (May 1955).

28. J. Bardeen, Phys. Rev., 49, 653 (1936).

29. D. Stark, Naturwiss., 48, 157 (1961).

30. M. Drechsler and R. Vannelow, Z. Krist., 107, 161 (1956).

31. W.R. Savage, Bull. Am. Phys. Soc., (2), 8, 198 (1963).

32. N.S. Rasor and C. Warner, AI-6799 First Summary Report for Contract Nonr-3192(00), November 15, 1961; C. Warner and N.S. Rasor, Bull. Am. Phys. Soc., (2), 7, 74 (1962).

33. M.H. Nichols, Phys. Rev., 57, 297 (1940).

34. R. Smoluchowski, Phys. Rev., 60, 661 (1941).

35. R.D. Young and E.W. Müller, J. Appl. Phys., 33, 91 (1962).

Contract No. AF-19(604)-8424
May 1963

DISTRIBUTION LIST

Code	Organization	No. of Copies
AF-2	A.U. (Library) Maxwell AFB, Alabama	1
AF-12	AWS (AWSSS/TIPD) Scott AFB, Illinois	1
AF-22	AFCRL, OAR (CRXR, Mr. John Marple) L.G. Hanscom Field Bedford, Massachusetts (U)	1
AF-23	AFCRL, OAR (CRXRA) Stop 39 L.G. Hanscom Field Bedford, Massachusetts	Please ship under separate cover as they must be sent to our Documents Unit. (20 cpys).
AF-26	AFCRL, OAR (CRZH, C.N. Touart) L.G. Hanscom Field Bedford, Massachusetts	1
AF-28	ESD (ESRDG) L.G. Hanscom Field Bedford, Massachusetts	1
AF-33	ACIC (ACDEL-7) Second and Arsenal St. Louis 18, Missouri (U)	1
AF-35	NAFEC Library Branch, Bldg. 3 Atlantic City, New Jersey ATTN: RD-702	1
AF-40	ASD (ASAPRD-Dist) Wright-Patterson AFB, Ohio	1
AF-43	Institute of Technology Library MCLI-LIB., Bldg. 125, Area B Wright-Patterson AFB, Ohio	1
AF-48	Hq. USAF (AFCSA, Secretary) Washington 25, D.C.	1

Code	Organization	No. of Copies
AF-49	AFOSR (SRGL) Washington 25, D.C.	1
AF-51	Hq. USAF (AFRDR) Washington 25, D.C.	1
AF-58	ARL (ARA-2) Library AFL 2292, Building 450 Wright-Patterson AFB, Ohio	1
AF-62	Hq. AFCRL, OAR (CRZWD, Irving I. Gringorton) L.G. Hanscom Field Bedford, Massachusetts	1
G-66	Scientific and Technical Information Facility ATTN: NASA Representative (S-AK-DL) P.O. Box 5700 Bethesda, Maryland	1
G-67	Office of Scientific Intelligence Central Intelligence Agency 2430 E Street, N.W. Washington 25, D.C.	1
AR-7	Commanding Officer U.S. Army Research and Development Laboratory Fort Monmouth, New Jersey	1
AR-13	Technical Documents Center Evans Signal Labs. Belmar, New Jersey	1
AR-15	Army Research Office Environmental Research Division 3045 Columbia Pike Arlington 4, Virginia	1
AR-16	Office of the Chief of Research and Dev. Department of the Army The Pentagon Washington 25, D.C.	1

Code	Organization	No. of Copies
F-7	Technical Information Office European Office, Aerospace Research Shell Building, 47 Cantersteen Brussels, Belgium (U)	1
F-50	Defense Research Member Canadian Joint Staff 2450 Massachusetts Ave., N.W. Washington 8, D.C. (U)	2
G-5	Librarian Boulder Laboratories National Bureau of Standards Boulder, Colorado (U)	1
G-21	ASTIA (TIPAA) Arlington Hall Station Arlington 12, Virginia	20
G-34	Documents Expediting Project (Unit X) Library of Congress Washington 25, D.C. (U)	1
G-40	Library National Bureau of Standards Washington 25, D.C. (U)	1
G-41	National Research Council 2101 Constitution Avenue Washington 25, D.C. (U)	1
G-47	Office of Secretary of (DDR and E, Tech. Library) Washington 25, D.C. (U)	1
G-49	Superintendent of Documents Government Printing Office Washington 25, D.C. (U)	1
G-51	Science Advisor Department of State Washington 25, D.C. (U)	1

Code	Organization	No. of Copies
G-52	Director of Meteorological Research U.S. Weather Bureau Washington 25, D.C.	1
G-53	Library U.S. Weather Bureau Washington 25, D.C.	1
I-7	Director, USAF Project RAND The Rand Corporation 1700 Main Street Santa Monica, California Thru A.F. Liaison Office	1
I-8	Dr. William W. Kellogg Rand Corporation 1700 Main Street Santa Monica, California (U)	1
I-40	Institute of Aerospace Sciences, Inc. 2 East 64th Street New York 21, New York (U)	1
I-46	Mr. Malcolm Rigby American Meteorological Society P.O. Box 1736 Washington 13, D.C. (U)	1
N-6	Technical Reports Librarian U.S. Naval Postgraduate School Monterey, California (U)	1
N-16	OAR (Geophysics Code N-416) Office of Naval Research Washington 25, D.C.	1
N-19	Director U S. Naval Research Laboratory Code 2027 Washington 25, D.C.	1

Code	Organization	No. of Copies
U-1	Library Geophysical Institute University of Alaska P.O. Box 938 College, Alaska (U)	1
U-10	Professor Clarence Palmer Institute of Geophysics University of California Los Angeles 24, California (U)	1
U-13	Dr. Joseph Kaplan Department of Physics University of California Los Angeles, California (U)	1
U-21	Dr. A.M. Peterson Stanford University Stanford, California (U)	1
U-40	Dr. David Fultz Department of Meteorology University of Chicago Chicago, Illinois (U)	1
U-56	Prof. Fred L. Whipple Harvard College Observatory 60 Garden Street Cambridge 38, Massachusetts (U)	1
	Remaining copies to: Hq. AFCRL, OAR (CRFE, Dr. Norman Rosenberg) L.G. Hanscom Field Bedford, Massachusetts	

UNCLASSIFIED

General Electric Research Laboratory, Schenectady, N. Y. THERMIONIC EMISSION FROM METAL CRYSTALS IN ALKALI METAL VAPORS, by H. F. Webster and P. L. Read. May 1963 54p. incl. illus. (Proj. 8659; Task 865902) (AFCRL-63-451) Scientific Report [Contract AF-19(604)-8424] Unclassified report

Thermionic emission microscopes have been used to evaluate the emission density from tungsten, molybdenum, tantalum, niobium, nickel, rhenium, and niobium carbide in cesium, rubidium, and potassium vapors as a function of alkali vapor pressure, emitter temperature, and emitter crystal face. It was found that when the emitter surface had less than a monolayer coverage of alkali metal, it was the atomically closest packed plane of the emitter which yielded the highest thermionic emission density. The effects of surface contaminants were studied and evidence was obtained suggesting that the high work function of the 112 plane of tungsten and molybdenum may be caused by a contaminant.

(over)

UNCLASSIFIED

UNCLASSIFIED

General Electric Research Laboratory, Schenectady, N. Y. THERMIONIC EMISSION FROM METAL CRYSTALS IN ALKALI METAL VAPORS, by H. F. Webster and P. L. Read. May 1963 54p. incl. illus. (Proj. 8659; Task 865902) (AFCRL-63-451) Scientific Report [Contract AF-19(604)-8424] Unclassified report

Thermionic emission microscopes have been used to evaluate the emission density from tungsten, molybdenum, tantalum, niobium, nickel, rhenium, and niobium carbide in cesium, rubidium, and potassium vapors as a function of alkali vapor pressure, emitter temperature, and emitter crystal face. It was found that when the emitter surface had less than a monolayer coverage of alkali metal, it was the atomically closest packed plane of the emitter which yielded the highest thermionic emission density. The effects of surface contaminants were studied and evidence was obtained suggesting that the high work function of the 112 plane of tungsten and molybdenum may be caused by a contaminant.

(over)

UNCLASSIFIED

UNCLASSIFIED

UNCLASSIFIED

UNCLASSIFIED

UNCLASSIFIED

General Electric Research Laboratory, Schenectady, N.Y. THERMIONIC EMISSION FROM METAL CRYSTALS IN ALKALI METAL VAPORS, by H. F. Webster and P. L. Read. May 1963 54p. incl. illus. (Proj. 8659; Task 865902)
(AFCRL-63-451) Scientific Report
[Contract AF-19(604)-8424]
Unclassified report

Thermionic emission microscopes have been used to evaluate the emission density from tungsten, molybdenum, tantalum,

(over)

UNCLASSIFIED

UNCLASSIFIED

General Electric Research Laboratory, Schenectady, N.Y. THERMIONIC EMISSION FROM METAL CRYSTALS IN ALKALI METAL VAPORS, by H. F. Webster and P. L. Read. May 1963 54p. incl. illus. (Proj. 8659; Task 865902)
(AFCRL-63-451) Scientific Report
[Contract AF-19(604)-8424]
Unclassified report

Thermionic emission microscopes have been used to evaluate the emission density from tungsten, molybdenum, tantalum,

(over)

UNCLASSIFIED

UNCLASSIFIED

niobium, nickel, rhenium, and niobium carbide in cesium, rubidium, and potassium vapors as a function of alkali vapor pressure, emitter temperature, and emitter crystal face. It was found that when the emitter surface had less than a monolayer coverage of alkali metal, it was the atomically closest packed plane of the emitter which yielded the highest thermionic emission density. The effects of surface contaminants were studied and evidence was obtained suggesting that the high work function of the 112 plane of tungsten and molybdenum may be caused by a contaminant.

UNCLASSIFIED

UNCLASSIFIED

niobium, nickel, rhenium, and niobium carbide in cesium, rubidium, and potassium vapors as a function of alkali vapor pressure, emitter temperature, and emitter crystal face. It was found that when the emitter surface had less than a monolayer coverage of alkali metal, it was the atomically closest packed plane of the emitter which yielded the highest thermionic emission density. The effects of surface contaminants were studied and evidence was obtained suggesting that the high work function of the 112 plane of tungsten and molybdenum may be caused by a contaminant.

UNCLASSIFIED

UNCLASSIFIED

General Electric Research Laboratory, Schenectady, N. Y. THERMIONIC EMISSION FROM METAL CRYSTALS IN ALKALI METAL VAPORS, by H. F. Webster and P. L. Read. May 1963 54p. incl. illus. (Proj. 8659; Task 865902)
(AFCRL-63-451) Scientific Report
[Contract AF-19(604)-8424]
Unclassified report

Thermionic emission microscopes have been used to evaluate the emission density from tungsten, molybdenum, tantalum,

(over)

UNCLASSIFIED

UNCLASSIFIED

General Electric Research Laboratory, Schenectady, N. Y. THERMIONIC EMISSION FROM METAL CRYSTALS IN ALKALI METAL VAPORS, by H. F. Webster and P. L. Read. May 1963 54p. incl. illus. (Proj. 8659; Task 865902)
(AFCRL-63-451) Scientific Report
[Contract AF-19(604)-8424]
Unclassified report

Thermionic emission microscopes have been used to evaluate the emission density from tungsten, molybdenum, tantalum,

(over)

UNCLASSIFIED

niobium, nickel, rhenium, and niobium carbide in cesium, rubidium, and potassium vapors as a function of alkali vapor pressure, emitter temperature, and emitter crystal face. It was found that when the emitter surface had less than a monolayer coverage of alkali metal, it was the atomically closest packed plane of the emitter which yielded the highest thermionic emission density. The effects of surface contaminants were studied and evidence was obtained suggesting that the high work function of the 112 plane of tungsten and molybdenum may be caused by a contaminant.

UNCLASSIFIED

UNCLASSIFIED

niobium, nickel, rhenium, and niobium carbide in cesium, rubidium, and potassium vapors as a function of alkali vapor pressure, emitter temperature, and emitter crystal face. It was found that when the emitter surface had less than a monolayer coverage of alkali metal, it was the atomically closest packed plane of the emitter which yielded the highest thermionic emission density. The effects of surface contaminants were studied and evidence was obtained suggesting that the high work function of the 112 plane of tungsten and molybdenum may be caused by a contaminant.

UNCLASSIFIED

UNCLASSIFIED

General Electric Research Laboratory, Schenectady, N.Y. THERMIONIC EMISSION FROM METAL CRYSTALS IN ALKALI METAL VAPORS, by H. F. Webster and P. L. Read. May 1963 54p. incl. illus. (Proj. 8659; Task 865902) (AFCRL-63-451) Scientific Report [Contract AF-19(604)-8424] Unclassified report

Thermionic emission microscopes have been used to evaluate the emission density from tungsten, molybdenum, tantalum, niobium, nickel, rhenium, and niobium carbide in cesium, rubidium, and potassium vapors as a function of alkali vapor pressure, emitter temperature, and emitter crystal face. It was found that when the emitter surface had less than a monolayer coverage of alkali metal, it was the atomically closest packed plane of the emitter which yielded the highest thermionic emission density. The effects of surface contaminants were studied and evidence was obtained suggesting that the high work function of the 112 plane of tungsten and molybdenum may be caused by a contaminant.

(over)

UNCLASSIFIED

UNCLASSIFIED

General Electric Research Laboratory, Schenectady, N.Y. THERMIONIC EMISSION FROM METAL CRYSTALS IN ALKALI METAL VAPORS, by H. F. Webster and P. L. Read. May 1963 54p. incl. illus. (Proj. 8659; Task 865902) (AFCRL-63-451) Scientific Report [Contract AF-19(604)-8424] Unclassified report

Thermionic emission microscopes have been used to evaluate the emission density from tungsten, molybdenum, tantalum, niobium, nickel, rhenium, and niobium carbide in cesium, rubidium, and potassium vapors as a function of alkali vapor pressure, emitter temperature, and emitter crystal face. It was found that when the emitter surface had less than a monolayer coverage of alkali metal, it was the atomically closest packed plane of the emitter which yielded the highest thermionic emission density. The effects of surface contaminants were studied and evidence was obtained suggesting that the high work function of the 112 plane of tungsten and molybdenum may be caused by a contaminant.

(over)

UNCLASSIFIED

UNCLASSIFIED